Cu-Au, Ag-Au, Cu-Ag, and Ni-Au intermetallics: First-principles study of temperature-composition phase diagrams and structures

V. Ozoliņš, C. Wolverton, and Alex Zunger
National Renewable Energy Laboratory, Golden, Colorado 80401
(Received 19 September 1997)

The classic metallurgical systems—noble-metal alloys—that have formed the benchmark for various alloy theories are revisited. First-principles fully relaxed general-potential linearized augmented plane-wave (LAPW) total energies of a few ordered structures are used as input to a mixed-space cluster expansion calculation to study the phase stability, thermodynamic properties, and bond lengths in Cu-Au, Ag-Au, Cu-Ag, and Ni-Au alloys. (i) Our theoretical calculations correctly reproduce the tendencies of Ag-Au and Cu-Au to form compounds and Ni-Au and Cu-Ag to phase separate at $T=0$ K. (ii) Of all possible structures, Cu_3Au ($L1_2$) and CuAu ($L1_0$) are found to be the most stable low-temperature phases of $Cu_{1-x}Au_x$ with transition temperatures of 530 K and 660 K, respectively, compared to the experimental values 663 K and ≈670 K. The significant improvement over previous first-principles studies is attributed to the more accurate treatment of atomic relaxations in the present work. (iii) LAPW formation enthalpies demonstrate that $L1_2$, the commonly assumed stable phase of $CuAu_3$, is *not* the ground state for Au-rich alloys, but rather that ordered (100) superlattices are stabilized. (iv) We extract the nonconfigurational (e.g., vibrational) entropies of formation and obtain large values for the size-mismatched systems: 0.48 k_B/atom in $Ni_{0.5}Au_{0.5}$ ($T=1100$ K), 0.37 k_B/atom in $Cu_{0.141}Ag_{0.859}$ ($T=1052$ K), and 0.16 k_B/atom in $Cu_{0.5}Au_{0.5}$ ($T=800$ K). (v) Using 8 atom/cell special quasirandom structures we study the bond lengths in disordered Cu-Au and Ni-Au alloys and obtain good qualitative agreement with recent extended x-ray-absorption fine-structure measurements.
[S0163-1829(98)08009-6]

I. INTRODUCTION: CHEMICAL TRENDS IN NOBLE-METAL ALLOYS

Noble-metal alloys are, experimentally, among the most studied intermetallic systems.[1–24] In addition, the Cu-Au system has been considered the classic paradigm system for applying different theoretical techniques of phase diagram and phase stability calculations.[25–63] Most notably, this system has been considered as the basic test case for the classic Ising-Hamiltonian statistical-mechanics treatment of alloys.[25–32] More recently, noble-metal binary alloys have been treated theoretically via empirical fitting of the constants in Ising Hamiltonians,[25–34] semiempirical interatomic potentials,[35–47] and via first-principles cluster expansions.[48–55] The essential difference in philosophy between the classical application of Ising models to CuAu (Refs. 25–30 and 33) and more modern approaches based on the density functional formalism[64] is that in the former approach the range and magnitudes of the interactions are postulated at the outset (e.g., first or second neighbor pair interactions), while the latter approaches make an effort to determine the interactions from an electronic structure theory. However, despite recent attempts,[48–54] it is still not clear whether the noble-metal alloys can be essentially characterized as systems with short-range pair interactions or not.

Now that first-principles cluster expansion approaches[65,66] have advanced to the stage where both $T=0$ ground state structures and finite-temperature thermodynamic quantities can be predicted without any empirical information, it is interesting to take a *global look* at the noble-metal alloy family. Table I summarizes some of the salient features[1–4,14,15,18,67–69] of the four binary systems Cu-Au, Ag-Au, Cu-Ag, and Ni-Au. We included the relative lattice constant mismatch $\Delta a/\bar{a}=2|a_A-a_B|/|a_A+a_B|$ between the constituents,[67] the electronegativity difference $\Delta\chi=\chi_A-\chi_B$ on the Pauling scale,[68] the mixing enthalpy of the equiatomic alloy,[2,18] the sign of the calculated nearest-neighbor pair interaction J_2 (present study), the structural identity of the low-temperature phases,[1–4,67] and the order-disorder transition (or miscibility gap) temperatures[2,69] T_c. Some interesting observations and trends, which we will attempt to reproduce theoretically, are apparent from this general survey.

(i) Despite a large (12%) size mismatch in Cu-Au and a small (≈0%) size mismatch in Ag-Au, *both* systems form ordered compounds at low temperatures and have negative mixing enthalpies, suggesting attractive (''antiferromagnetic'') *A-B* interactions. Thus, when the difference in the electronegativity, $\Delta\chi$, of the constituent atoms is sufficiently large, as it is in CuAu and AgAu, size mismatch apparently does not determine ordering vs phase separation tendencies.

(ii) Despite a similar size mismatch (12%) in Cu-Au and Cu-Ag, the former orders while the latter phase separates. Thus, the existence of a large electronegativity difference in Cu-Au (as opposed to the small difference in Cu-Ag) seems to induce ordering tendencies.

(iii) Cu-Ag and Ni-Au both phase separate (and have positive ΔH_{mix}) as they have large size mismatches. Yet, Ni-Au, having a large electronegativity difference, shows an ordering-type nearest-neighbor pair interaction ($J_2>0$), just like the compound forming Cu-Au and Ag-Au, while Cu-Ag has a clustering-type nearest-neighbor interaction ($J_2<0$). Thus, the sign of J_2 does not reflect the low-temperature ordering vs phase separation.

 © 1998 The American Physical Society

TABLE I. Major physical properties of Ag-Au, Cu-Ag, Cu-Au, and Ni-Au alloys. We give constituent size mismatches $\Delta a/\overline{a}=2(a_A-a_B)/(a_A+a_B)$, electronegativity differences on the Pauling scale (Ref. 68) $\Delta\chi$, mixing enthalpies of the disordered alloys at the equiatomic composition, $\Delta H_{\rm mix}(x=\frac{1}{2})$, signs of the nearest-neighbor Ising interaction, J_2, order-disorder transition temperatures (or miscibility gap temperatures for Cu-Ag and Ni-Au) $T_c(x=\frac{1}{2})$, and excess entropies of solid solutions, $\Delta S_{\rm tot}^{\rm form}-\Delta S_{\rm ideal}$. All phases are fcc based.

System	$\Delta a/\overline{a}$ [a]	$\Delta\chi$ [b]	$\Delta H_{\rm mix}(x=1/2)$ (meV/atom)	J_2	Low-T phases [g]	$T_c(x=\frac{1}{2})$ (K)	$\Delta S_{\rm tot}^{\rm form}-\Delta S_{\rm ideal}$ [g] (k_B/atom)
Cu-Au	12%	0.64	-91 [c]	>0	$L1_2$, $L1_0$, $L1_2$(?)	683 [g]	$+0.04$
Ag-Au	0%	0.61	-48 [d]	>0	$L1_2$, $L1_0$, $L1_2$	115-168 [h]	-0.17
Cu-Ag	12%	0.03	$+104$ [e]	<0	Phase sep.	$>T_m$	$+0.36$
Ni-Au	15%	0.63	$+76$ [f]	>0	Phase sep.	1083 [d]	$+0.35$

[a]Ref. 67.
[b]Ref. 68.
[c]Refs. 15, 14, and 2.
[d]Ref. 2.
[e]Theoretically calculated value from this work.
[f]Refs. 2 and 18.
[g]Refs. 2 and 4.
[h]Ref. 69.

(iv) The amount $\Delta S_{\rm XS}=\Delta S_{\rm tot}^{\rm expt}-\Delta S_{\rm ideal}$ by which the measured entropy[2] $\Delta S_{\rm tot}^{\rm expt}$ deviates from the ideal configurational entropy $\Delta S_{\rm ideal}=k_B[x\ln x+(1-x)\ln(1-x)]$ is unexpectedly large in Cu-Ag and Ni-Au, indicating a large nonconfigurational entropy of formation.

Other interesting facts about the noble-metal binary intermetallics include the following.

(v) Despite numerous studies,[1–4,7,8,10–12] the structure of the ordered phases in Au-rich Cu-Au is not well established yet. It is often assumed[1–4] that the stable Au-rich low-temperature phase is $CuAu_3$ in the $L1_2$ structure, but direct experiments[7,8,10] below the order-disorder transition temperature $T_c(x=\frac{3}{4})\approx 500$ K are difficult because the diffusion rates are very low and even the best ordered samples contain significant disorder. Possible further thermodynamic transformations at lower temperatures may be kinetically inhibited.

(vi) The trends in bond lengths vs composition are nontrivial. Traditionally, all coherent-potential-approximation-based theories[70–72] of intermetallic alloys have assumed that the nearest-neighbor bond lengths are equal, $R_{AA}=R_{AB}=R_{BB}$, and proportional to the average lattice constant. Recent theories[73–75] suggested, however, that bond lengths relax in the alloy to new values, and this has a significant effect on the electronic structure.[53,76,77] Recent extended x-ray-absorption fine-structure (EXAFS) experiments on NiAu (Ref. 23) and CuAu (Ref. 24) show distinct $R_{AA}\neq R_{AB}\neq R_{BB}$ bond lengths, which need to be explained.

In this work we will analyze the above-mentioned trends in terms of a first-principles mixed-space cluster expansion,[65,66] based on modern local density approximation (LDA) total energy calculations. We reproduce the observed trends (i)–(vi) in ordering preferences, mixing enthalpies $\Delta H_{\rm mix}$, transition temperatures T_c, and interatomic bond lengths. In addition, we predict new, and to our knowledge hitherto unsuspected, ordered phases in Au-rich Cu-Au alloys.

II. BASIC IDEOLOGY AND METHODOLOGY

There are many problems in solid state physics that require knowledge of the total energy $E(\sigma)$ of a lattice with N sites as a function of the occupation pattern σ of these sites by atoms of types A and B. This information is needed, for example, in the ground state search problem,[72] where one seeks the configuration with the lowest energy at $T=0$ K. $\{E(\sigma)\}$ is also needed for calculating the temperature- and composition-dependent thermodynamic functions and phase diagrams of an $A_{1-x}B_x$ alloy.

A direct, quantum-mechanical calculation of the total energy $E_{\rm direct}(\sigma)=\langle\Psi|\hat{H}|\Psi\rangle/\langle\Psi|\Psi\rangle$ (where Ψ is the electronic ground state wave function and $\hat{H}$ is the many-electron Hamiltonian) is possible only for a limited set of configurations σ. This is so because (i) the computational effort to solve the Schrödinger equation for a single configuration scales as the cube of the number of atoms per unit cell, so that only small unit cells can be considered, (ii) there are 2^N configurations, and (iii) for each configuration, one has to find the atomic relaxations $\delta\mathbf{u}_{\rm min}(\sigma)$ which minimize the total energy. Consequently, one searches for a ''cluster expansion'' (CE) that accurately reproduces the results of a direct, quantum-mechanical (e.g., LDA) calculation,

$$E_{\rm CE}(\sigma)\cong E_{\rm direct}(\sigma), \tag{1}$$

without the unfavorable scaling of the computational cost with the size of the unit cell.

In designing a cluster expansion, there are few choices of independent parameters. For example, one could choose to obtain a cluster expansion for the volume- (V-) dependent equation of state $E_{\rm direct}(\sigma,V)$ [see, e.g., Refs. 52, 78, and 79] or to find a cluster expansion for the energy at the volume $V_{\rm min}(\sigma)$ that minimizes $E_{\rm direct}(\sigma,V)$. We choose the latter possibility. Furthermore, for each configuration σ, we wish to reproduce the total energy corresponding to the fully re-

laxed cell shape and atomic positions $\{\delta\mathbf{u}_{\min}(\sigma)\}$. In other words, we choose to represent

$$E_{\rm CE}(\sigma)\cong E_{\rm direct}[\sigma;\delta\mathbf{u}_{\min}(\sigma);V_{\min}(\sigma)]\equiv E_{\rm direct}(\sigma). \quad (2)$$

Note that by focusing on the equilibrium energy of each configuration, we give up the possibility of studying nonequilibrium geometries (e.g., bond lengths) and equations of state. Instead, for each occupation pattern σ, we can find the total energy $E(\sigma)$ of the atomically relaxed and volume-optimized geometry.

The best-known cluster expansion is the generalized Ising model in which the equilibrium total energy of an *arbitrary* configuration σ is expanded in a series of basis functions defined as pseudospin products on the crystal sites:

$$E(\sigma)=J_0+\sum_i J_iS_i+\frac{1}{2}\sum_{i\neq j} J_{ij}S_iS_j + \frac{1}{3!}\sum_{i\neq j\neq k} J_{ijk}S_iS_jS_k+\cdots, \quad (3)$$

where in binary $A_{1-x}B_x$ alloys $S_i=+1$ or -1, depending on whether the site i is occupied by an atom of type A or B. Equation (3) is valid whether the lattice is relaxed or not, as long as a one-to-one correspondence exists between the actual positions of atoms and the ideal fcc sites. The practical usefulness of the cluster expansion, Eq. (3), rests on the assumption that the effective cluster interactions (ECI's), $J_{ij}, J_{ijk}, \ldots$, are rapidly decreasing functions of the number of sites and intersite separation, so that only a finite number of terms has to be kept in Eq. (3) for the desired accuracy. In this case, we can write the formation enthalpy of structure σ,

$$\Delta H_{\rm direct}(\sigma)=E(\sigma)-xE_A-(1-x)E_B, \quad (4)$$

where E_A and E_B are total energies of the pure constituents A and B, as the following CE:

$$\Delta H_{\rm CE}(\sigma)=J_0+\sum_f^{N_f} D_f\,J_f\overline{\Pi}_f(\sigma). \quad (5)$$

Here N_f is the number of nonzero effective interactions, D_f is the number of clusters of type f per lattice site, and $\overline{\Pi}_f(\sigma)$ are lattice averages of the spin products in configuration σ.

Sanchez, Ducastelle, and Gratias[80] have shown that there is a set of composition-independent interactions for Eq. (3) which can exactly reproduce the directly calculated total energies of *all* configurations σ. This statement is strictly true if all possible clusters are included in Eq. (3), and should hold for the truncated series, Eq. (3), if the cluster expansion is well converged. Several methods[81,82] yield concentration-dependent effective interactions, providing in principle equally valid schemes for representing $\Delta H_{\rm direct}(\sigma)$ in terms of a cluster expansion. In the present work, we select composition-independent interactions, since these can be directly compared to previous Ising model treatments[25–34,48–55] of the noble-metal alloy phase diagrams.

A number of issues arise in trying to construct a cluster expansion that satisfies Eq. (2).

(i) The number of interactions and their types (pair, multibody) cannot be decided arbitrarily, but must be constrained by a microscopic electronic-structure theory according to Eqs. (1) and (2).

(ii) In most configurations σ, atoms move away from the ideal lattice sites, which not only lowers the total energies $E_{\rm direct}(\sigma)$, but also slows down the convergence[85] of the expansion, Eq. (3). The solution is to have a cluster expansion with many interaction terms N_J that can represent such situations. We accomplish this by using a reciprocal-space formulation, formally equivalent to an infinite number of real-space pair interactions.

(iii) Some cluster expansions[78] require that the number of interactions, N_J, must equal the number of configurations, N_σ, whose total energies need to be evaluated via the direct electronic-structure method. The number of such calculations may be excessive in view of (ii). We thus introduce a method in which $N_\sigma \ll N_J$. Furthermore, interactions that are not needed to satisfy Eq. (2) are automatically discarded.

(iv) One has to deal with the macroscopic elastic strain leading to a $\mathbf{k}\to 0$ singularity in the Fourier transform of the pair interactions,

$$J_{\rm pair}(\mathbf{k})=\sum_j J_{\rm pair}(\mathbf{R}_i-\mathbf{R}_j)e^{-i\mathbf{k}\cdot\mathbf{R}_j}. \quad (6)$$

As shown by Laks *et al.*[65] (see also the discussion below), in size-mismatched systems the correct $J_{\rm pair}(\mathbf{k})$ depends on direction $\hat{k}$ in the long-wavelength limit $\mathbf{k}\to 0$. To solve this, we express $J_{\rm pair}(\mathbf{k})$ as a sum of two parts,

$$J_{\rm pair}(\mathbf{k})=J_{\rm SR}(\mathbf{k})+J_{\rm CS}(\hat{k}), \quad (7)$$

where $J_{\rm SR}(\mathbf{k})$ is an analytic function of $\mathbf{k}$ and can be obtained from short-ranged real-space pair interactions, while $J_{\rm CS}(\hat{k})$ contains the nonanalytic behavior around $\mathbf{k}=0$ and depends only on the direction $\hat{k}$. To explain this singularity, we consider the energy of a coherent A_nB_n superlattice, formed by a periodic stacking of n layers of A and n layers of B in direction $\hat{G}$. By introducing the structure factor

$$S(\mathbf{k},\sigma)=\sum_j S_je^{-i\mathbf{k}\cdot\mathbf{R}_j}, \quad (8)$$

the total pair interaction energy in Eq. (3) can be expressed as a reciprocal-space sum:

$$E_{\rm pair}(\sigma)=\sum_{\mathbf{k}} J_{\rm pair}(\mathbf{k})\,|S(\mathbf{k},\sigma)|^2. \quad (9)$$

The A_nB_n superlattice has a nonzero structure factor at $\mathbf{k}=(1/2n)\hat{G}$, and therefore its energy is determined by $J_{\rm pair}[(1/2n)\hat{G}]$. As $n\to\infty$ its formation energy is given by a sum of the epitaxial deformation energies of pure constituents needed to bring them to a common lattice constant in the plane perpendicular to $\hat{G}$. Since the epitaxial deformation energy of pure constituents is direction dependent (e.g., it is easier to stretch Cu in [100] planes than in [111] planes; see Sec. III B), the formation energy $\Delta H(A_\infty B_\infty)$ is also direction dependent. Therefore, $\lim_{\mathbf{k}\to 0}J_{\rm pair}(\mathbf{k})$ must depend on the direction of approach to the origin, proving that $J_{\rm pair}(\mathbf{k})$

is singular. Physically, the nonanaliticity of $J_{\rm pair}(\mathbf{k})$ is caused by long-range interactions via macroscopic elastic strain and cannot be reproduced using finite-ranged real-space pair interactions, but must be accounted for explicitly in reciprocal space. If the singularity is neglected, then as explained in Ref. 65, the cluster expansion fails not only for long-period ($n\to\infty$) superlattices A_nB_n, but also for those short-period ($n>2$) superlattices which have not been explicitly included in the constraint, Eq. (2). We emphasize that although the contribution of $J_{\rm CS}(\mathbf{k})$ to the formation energy is nonzero only in size-mismatched systems, it is not related to the atomic relaxation energy for a particular structure σ in any simple way (except if σ itself is a long-period superlattice).

The singularity in $J_{\rm pair}(\mathbf{k})$ is similar to the singularity in the dynamical matrix $D_{\alpha\beta}(\kappa\kappa'|\mathbf{k})$ of polar crystals in the long-wavelength limit,[83] caused by long-range electrostatic interactions via macroscopic electric field. In lattice dynamics, $D_{\alpha\beta}(\kappa\kappa'|\mathbf{k})$ is expressed as a sum of regular and singular parts, $D_{\alpha\beta}(\kappa\kappa'|\mathbf{k})=D^{\rm sing}_{\alpha\beta}(\kappa\kappa'|\mathbf{k})+D^{\rm reg}_{\alpha\beta}(\kappa\kappa'|\mathbf{k})$, where $D^{\rm reg}_{\alpha\beta}(\kappa\kappa'|\mathbf{k})$ (analytic as $\mathbf{k}\to 0$) is due to short-range force constants. The singular part $D^{\rm sing}_{\alpha\beta}(\kappa\kappa'|\mathbf{k})$ gives rise to LO/TO splitting of the zone-center optical frequencies ω_Γ in polar crystals, and also leads to a directional dependence of $\omega_\Gamma(\hat{k})$ in uniaxial crystals (e.g., CuPt-type $GaInP_2$). These phenomena cannot be reproduced by any set of finite-ranged microscopic force constants, but have to be calculated explicitly using the macroscopic Maxwell equations.[84]

In summary, we seek to find a function $E_{\rm CE}(\sigma)$ which accurately reproduces the LDA total energies $E_{\rm LDA}[\sigma,\delta\mathbf{u}_{\rm min}(\sigma);V_{\rm min}(\sigma)]\equiv E_{\rm LDA}(\sigma)$ at the atomically relaxed geometry and equilibrium volume of configuration σ. The function $E_{\rm CE}(\sigma)$ we consider includes composition- and volume-independent interactions, so as to maintain maximum similarity with the classical Ising model. The number and type of interactions are not decided arbitrarily, but are constrained by the electronic-structure theory used (here, the LDA). Relaxation is treated accurately by including long-range pair interactions in the reciprocal-space representation. The $\mathbf{k}\to 0$ singularity, affecting both short- and long-period superlattices, is dealt with explicitly.

The above requirements are satisfied by the mixed-space cluster expansion (MSCE)

$$\Delta H_{\rm CE}(\sigma)=\sum_{\mathbf{k}} J_{\rm pair}(\mathbf{k})\ |S(\mathbf{k},\sigma)|^2 + \sum_{f}^{\rm MB} D_f\ J_f\overline{\Pi}_f\ (\sigma)+\Delta E_{\rm CS}(\sigma). \qquad (10)$$

We have separated out the so-called equilibrium constituent strain energy term $\Delta E_{\rm CS}(\sigma)$, which accounts for the $\mathbf{k}\to 0$ singularity.[65] In Eq. (10) we do not need to calculate $\Delta E_{\rm CS}(\sigma)$ for each configuration σ, but only for the *directions* $\hat{k}$ of the wave vectors with nonzero $S(\mathbf{k},\sigma)$. In fact, it is constructed to coincide with the elastic strain energy of coherent superlattices in the long-period limit:[65]

$$\Delta E_{\rm CS}(\sigma)=\sum_{\mathbf{k}} J_{\rm CS}(x,\hat{k})|S(\mathbf{k},\sigma)|^2, \qquad (11)$$

$$J_{\rm CS}(x,\hat{k})=\frac{\Delta E^{\rm eq}_{\rm CS}(x,\hat{k})}{4x(1-x)}, \qquad (12)$$

where $S(\mathbf{k},\sigma)$ is the structure factor from Eq. (8). The quantity $\Delta E^{\rm eq}_{\rm CS}(x,\hat{k})$ depends only on the direction $\hat{k}$, and will be given in Sec. III B. Equation (11) is *exact* for long-period superlattices, but represents a *choice* for short-period superlattices and nonsuperlattice (e.g., $L1_2$) structures. It has been found[65] that the choice, Eq. (11), improves the cluster expansion predictions also for short-period superlattices.

Equation (10) is a generalized Ising model description of the formation energy of *any* relaxed configuration σ, even if a direct LDA calculation for this σ is impractical. The cluster interaction energies $\{J_{\rm pair}(\mathbf{k})\}$ and $\{J_f\}$ are obtained by fitting Eq. (10) to the LDA formation energies. An additional smoothness requirement is imposed on $J_{\rm pair}(\mathbf{k})$, which ensures that the pair interactions are optimally short ranged in real space. Namely, we minimize the sum,

$$\Delta^2_{\rm rms}=\frac{1}{N_\sigma}\sum_{\sigma} w_\sigma[\Delta H_{\rm CE}(\sigma)-\Delta H_{\rm LDA}(\sigma)]^2 + \frac{t}{\alpha}\sum_{\mathbf{k}} J_{\rm pair}(\mathbf{k})[-\nabla^2_{\mathbf{k}}]^{\lambda/2}J_{\rm pair}(\mathbf{k}), \qquad (13)$$

where λ and t are free parameters and α is a normalization constant.[65] Typically we choose $\lambda=4$ and $t=1$, but the fit is not sensitive to this choice.

This approach solves the four problems indicated above in the sense that (i) the fitting process itself automatically selects the pair interactions that are essential to obtain a good fit (process still does not select multibody figures), (ii) the pair interactions can be of arbitrary long range, facilitating treatment of systems with large elastic relaxations, (iii) the number of pairs can be much larger than the number of ordered structures in the fit, and (iv) the directly calculated constituent strain energy $\Delta E_{\rm CS}$ contains the $\mathbf{k}\to 0$ singularity. Unlike all coherent-potential-approximation- (CPA-) based methods,[70,71] the present approach includes a full account of atomic relaxation and local environment effects. Unlike the classical Ising descriptions,[25,27–33] the interaction energies are determined by the electronic structure rather than being guessed. Finally, unlike the computational alchemy linear response approach,[85] multibody terms are included here.

Having written the expression for the total energy of arbitrary configuration, Eq. (10), we can evaluate its constants from a limited number of LDA calculations on small unit cell ($N_{\rm atoms}<10$) ordered structures with fully relaxed atomic positions. Equation (10) can then be employed in simulated annealing and Monte Carlo calculations[86,87] yielding $T=0$ ground states and $T>0$ statistical and thermodynamic properties. Further details of the method are given in Sec. III.

III. DETAILS OF THE METHOD

A. $T=0$ energetics

The calculations of $T=0$ total energies employ the full-potential linearized augmented plane wave (FLAPW) method[88]. The basis set consists of plane waves in the interstitial region, augmented in a continuous and differentiable way with the solutions of the radial Schrödinger equation inside the nonoverlapping muffin-tin spheres. Nonspherical

potential and electronic charge density terms are calculated in all space and included in the Hamiltonian matrix. Core states are treated fully relativistically and recalculated in each self-consistency iteration. The wave equation for the valence states includes all relativistic effects except the spin-orbit interaction; i.e., they are treated scalar relativistically. The FLAPW method is the most accurate all-electron method, superior to the methods employing overlapping atomic spheres [atomic-sphere approximation (ASA)] and/or shape approximations to the potential.

We use the Wigner exchange-correlation functional.[89] As a check, we have performed several calculations using the Perdew-Zunger[90] parametrization of the Ceperley-Alder[91] functional and the generalized gradient approximation of Perdew and Wang.[92] We find (see Sec. IV A 1) that the various exchange-correlation functionals change the enthalpies of formation of ordered Cu-Au compounds by a negligible amount (less than 2 meV/atom).

The total energies of the ordered structures and end-point constituents are obtained keeping all computational parameters exactly equal. Specifically, we always use the same basis sets ($RK_{\max}=9$), charge density cutoffs ($RK_{\max}=19$), muffin-tin radii $R_{\mathrm{Au}}=2.4a_0$, $R_{\mathrm{Ag}}=R_{\mathrm{Cu}}=R_{\mathrm{Ni}}=2.2a_0$, maximum difference in the angular momenta in the nonspherical Hamiltonian terms ($l_{\max}=4$), maximum angular momenta in the nonspherical charge densities and potentials inside the muffin-tin spheres ($l_{\max}=8$), and equivalent **k** point sets[93] in the evaluation of Brillouin zone integrals. When the unit cell vectors of the ordered compound permit, we choose a **k** mesh equivalent to the 60 special points $8\times8\times8$ fcc mesh. Several structures (e.g., those of A_2B or AB_2 stoichiometry) have reciprocal unit cell vectors which are incommensurate with the $8\times8\times8$ mesh. In these cases we calculate the total energies of the compounds *and* fcc constituents with a finer **k** point grid. This procedure ensures that, due to systematic cancellation of errors, the formation enthalpies $\Delta H(\sigma)$, Eq. (4), converge much faster than the total energies. Indeed, the tests for Cu-Au described in Sec. IV A 1 show that with our choice of parameters $\Delta H(\sigma)$ are converged to within 2 meV/atom.

The atomic positions are relaxed using quantum-mechanical forces[94] obtained at the end of the self-consistency iterations. Minimization of the total energy with respect to the cell-external degrees of freedom is done by distorting the shape of the unit cell and tracing the decrease in the total energy. We estimate that the formation enthalpies are converged to at least 5 meV/atom with respect to all relaxational degrees of freedom.

Table II and its caption defines our small-unit-cell ordered structures. Many are actually superlattices along (100), (110), (111), (201), and (311) directions. Table III gives the calculated LDA formation energies [Eq. (4)] for these Au-Ag, Cu-Au, Cu-Ag, and Ni-Au compounds.

B. Constituent strain energy

It is well known[66] that real-space cluster expansions with finite-ranged interactions incorrectly predict zero formation enthalpies per atom for coherent long-period A_pB_q superlattices, while the correct answers are nonzero and depend on the superlattice direction $\hat{G}$. The constituent strain energy term $\Delta E_{\mathrm{CS}}(\sigma)$ in Eq. (10) is specifically designed to reproduce these superlattice energies, which are calculated directly from the LDA as follows.

In the long-period limit $pq\to\infty$ the interfacial energy becomes negligibly small $[\mathcal{O}(1/p)]$ in comparison with the elastic strain energy needed to deform the constituents to a common in-plane lattice constant a_s.[55,96] Therefore, the formation energy per atom of $A_\infty B_\infty$ superlattice along $\hat{G}$ with composition x is given by the constituent strain energy $\Delta E_{\mathrm{CS}}(x,\hat{G})$, defined as the equilibrium (eq) value of the composition-weighted sum of the energies required to deform bulk A and B to the epitaxial geometry with a planar lattice constant a_s:

$$\Delta E^{\mathrm{eq}}_{\mathrm{CS}}(x,\hat{G})=\min_{a_s}[x\Delta E^{\mathrm{epi}}_{\mathrm{A}}(a_s,\hat{G})+(1-x)\Delta E^{\mathrm{epi}}_{\mathrm{B}}(a_s,\hat{G})]. \tag{14}$$

Here $\Delta E^{\mathrm{epi}}(a_s,\hat{G})$ is the strain energy of the material epitaxially stretched to the lattice constant a_s in the direction orthogonal to $\hat{G}$, and then allowed to relax along $\hat{G}$. $\Delta E^{\mathrm{epi}}(a_s,\hat{G})$ is related to the bulk equation of state $\Delta E^{\mathrm{bulk}}(a_s)$ via the epitaxial softening function $q(a_s,\hat{G})$:

$$q(a_s,\hat{G})\equiv\frac{\Delta E^{\mathrm{epi}}(a_s,\hat{G})}{\Delta E^{\mathrm{bulk}}(a_s)}, \tag{15}$$

where $\Delta E^{\mathrm{bulk}}_A(a_s)$ is the energy required to hydrostatically deform a bulk solid to the lattice constant a_s. Figure 1 illustrates the concept of epitaxial softening:[97] When the bulk solid is deformed hydrostatically from a_{eq} to $a_s\neq a_{\mathrm{eq}}$, its energy rises. The energy can then be lowered if we keep $a_x=a_y=a_s$ but relax the third lattice vector to its equilibrium value. $q(a_s,\hat{G})$ measures the relative energy lowering.

Figure 2 shows the calculated LDA q's for Cu, obtained by minimizing the total energy with respect to the lattice constant c parallel to $\hat{G}$ for each value of the substrate lattice parameter a_s. As explained in Ref. 96, this treatment neglects the so-called shear strain terms, but is exact for the high-symmetry directions (100), (111), and (110). The calculated $q_{\mathrm{Cu}}(a_s,\hat{G})$ is seen to be a nontrivial function of the substrate lattice parameter a_s and direction $\hat{G}$. In contrast, the harmonic elasticity theory,[97–102] routinely used for semiconductor systems,[97,100,101] gives q's which do not depend on a_s,

$$q_{\mathrm{harm}}(\hat{G})=1-\frac{B}{C_{11}+\Delta\gamma_{\mathrm{harm}}(\hat{G})}, \tag{16}$$

where $\gamma_{\mathrm{harm}}(\hat{G})$ is a geometric function of the spherical angles formed by $\hat{G}$:

$$\gamma_{\mathrm{harm}}(\phi,\theta)=\sin^2(2\theta)+\sin^4(\theta)\sin^2(2\phi)$$
$$=\frac{4}{5}\sqrt{4\pi}\left[K_0(\phi,\theta)-\frac{2}{\sqrt{21}}K_4(\phi,\theta)\right], \tag{17}$$

and K_l are the Kubic harmonics of angular momentum l. Figure 2 shows that the harmonic approximation manifestly breaks down for large epitaxial strains in metals since there

TABLE II. Definition of the small-unit-cell ordered structures used in the LDA total energy calculations.

Simple superlattices					
Composition	Orientation				
	(001)	(011)	(111)	(311)	(201)
AB	$L1_0$ (CuAu)	$L1_0$ (CuAu)	$L1_1$ (CuPt)	$L1_1$ (CuPt)	$L1_0$ (CuAu)
A_2B	''$\beta 1$'' ($MoSi_2$)	''$\gamma 1$'' ($MoPt_2$)	''$\alpha 1$'' (CdI_2)	''$\gamma 1$'' ($MoPt_2$)	''$\gamma 1$''($MoPt_2$)
AB_2	''$\beta 2$'' ($MoSi_2$)	''$\gamma 2$'' ($MoPt_2$)	''$\alpha 2$'' (CdI_2)	''$\gamma 2$'' ($MoPt_2$)	''$\gamma 2$''($MoPt_2$)
A_3B	''$Z1$''	''$Y1$''	''$V1$''	''$W1$''	$D0_{22}$ ($TiAl_3$)
AB_3	''$Z3$''	''$Y3$''	''$V3$''	''$W3$''	$D0_{22}$ ($TiAl_3$)
A_2B_2	''$Z2$''	''$Y2$''	''$V2$''	''$W2$''	''40''($CuFeS_2$)

Other structures					
Composition	Name	Prototype	Superlattice direction	Period	Reference
A_3B_1	$L1_2$	Cu_3Au	none		52
A_1B_3	$L1_2$	Cu_3Au	none		52
A_7B	$D7_a$		none		52
A_4B_4	$D4$		none		52
AB_7	$D7_b$		none		52
A_8B		Ni_8Nb	none		95
AB_8		Ni_8Nb	none		95
A_6B_2	$D0_{23}$	Al_3Zr	(401)	(5,1,1,1)	95
A_6B_2	LPS-3		(601)	(5,1,1,1)	87
A_4B_4	$SQS8_a$		(311)	(2,3,2,1)	76
A_4B_4	$SQS8_b$		(311)	(3,2,1,2)	76
A_6B_2	$SQS14_a$		(201)	(6,2)	73
A_2B_6	$SQS14_b$		(201)	(2,6)	73

are several important *qualitative* differences between the behavior in Fig. 2 and that predicted by the harmonic elasticity. First, $q(a_s,\hat{G})$ strongly depends on the substrate lattice constant, while the harmonic $q_{\rm harm}(\hat{G})$ does not. Second, the harmonic expression gives a definite order of $q(\hat{G})$ as a function of the direction; i.e., either (100) is the softest and then (111) *must* be the hardest, or vice versa. This order does not hold for large deformations. For instance, (201) becomes the softest direction for $a_s \ll a_0$ and (110) is the hardest for $a_s \gg a_0$ in Cu. Finally, $q(100)$ exhibits a particularly dramatic softening for $a_s \gg a_0$, which has important consequences for the constituent strain energy and stability of superlattices along this direction.[96]

The above-mentioned properties of $q_{\rm Cu}$ can be described by generalizing Eq. (17) for γ to higher Kubic harmonics and strain-dependent expansion coefficients:

$$\gamma(a_s,\hat{G}) = \sum_{l=0}^{l_{\max}} b_l(a_s)\ K_l(\hat{G}), \tag{18}$$

which has the property that in the harmonic limit ($a_s \to a_0$) all expansion coefficients with angular momenta higher than 4 tend to zero, reproducing $\gamma_{\rm harm}$ from Eq. (17). Due to the cubic symmetry, only terms with $l=0,4,6,8,10,12,\ldots$ enter in this expansion. A detailed discussion of the nonlinear epitaxial strain properties of elemental metals will be given in a separate publication.[96]

The constituent strain energy $\Delta E^{\rm eq}_{\rm CS}(x,\hat{G})$ is calculated numerically from Eq. (14) using the direct LDA values of $\Delta E^{\rm epi}(a_s,\hat{G})$ for six principle directions. The obtained $\Delta E^{\rm eq}_{\rm CS}$ for these directions are shown in Fig. 3, illustrating several properties of the constituent strain which cannot be reproduced by the harmonic theory.[65] First, the curves in Fig. 3 are skewed to different sides, while the harmonic $\Delta E^{\rm eq}_{\rm CS}$ must be all skewed to the same side. Second, the calculated $\Delta E^{\rm eq}_{\rm CS}$ cross for different directions, a property not allowed by the harmonic functional form. These crossings lead to (201) as the softest direction below $x \approx 0.2$ and (110) as the hardest for Au-rich superlattices, while the harmonic theory gives $\Delta E^{\rm eq}_{\rm CS}(111)$ as the highest and $\Delta E^{\rm eq}_{\rm CS}(100)$ as the lowest constituent strain for all compositions of the studied noble-metal alloys. The behavior of $\Delta E^{\rm eq}_{\rm CS}$ for (100) is particularly interesting, since the curves in Fig. 3 abruptly change slope around $x \approx 0.15$ and have very low values for $x > \frac{1}{4}$. As we show in Ref. 96, this is a manifestation of the low energy cost of deforming fcc Cu into the body-centered tetragonal structure along the epitaxial Baines path. A small constituent strain of (100) superlattices has a profound influence on the predicted ground states of Cu-Au (see Sec. IV A 1).

The constituent strain energy for arbitrary direction $\hat{G}$ is then obtained by interpolating between the principle directions using the following expansion in Kubic harmonics:

$$\Delta E_{\rm CS}(x,\hat{G}) = \sum_{l=0}^{l_{\max}} c_l(x)\ K_l(\hat{G}). \tag{19}$$

TABLE III. LDA calculated formation [Eq. (4)] enthalpies for fcc superstructures (defined in Table II) of Ag-Au, Cu-Ag, Cu-Au, and Ni-Au. The numbers in parentheses represent errors of the cluster expansion fit. All energies in meV/atom.

Structure		Ag-Au	Cu-Ag		Cu-Au		Ni-Au	
Superlattice	Name	$\Delta H^{\mathrm{LDA}}_{\mathrm{unrel}}$	$\Delta H^{\mathrm{LDA}}_{\mathrm{unrel}}$	$\Delta H^{\mathrm{LDA}}_{\mathrm{rel}}$	$\Delta H^{\mathrm{LDA}}_{\mathrm{unrel}}$	$\Delta H^{\mathrm{LDA}}_{\mathrm{rel}}$	$\Delta H^{\mathrm{LDA}}_{\mathrm{unrel}}$	$\Delta H^{\mathrm{LDA}}_{\mathrm{rel}}$
A	fcc	0.0(−0.4)	0.0	0.0(−0.1)	0.0	0.0(+0.2)	0.0	0.0(+0.4)
B	fcc	0.0(−0.5)	0.0	0.0(+0.3)	0.0	0.0(−0.4)	0.0	0.0(−0.2)
(001) Structures								
AB	$L1_0$	−59.7(−0.8)	+107.6	+100.5(+0.4)	−36.1	−48.2(+0.1)	+98.1	+76.1(+1.4)
A_2B	''$\beta 1$''	−40.8(−0.1)	+130.2	+90.8(−0.7)	+51.0	−3.8(−2.6)	+207.8	+105.7(−0.1)
AB_2	''$\beta 2$''	−40.0(+0.1)	+112.0	+75.0(+1.0)	+40.1	−40.8(+0.6)	+151.7	+38.3(+0.1)
A_3B	''$Z1$''	−29.2(−0.1)	+126.4	+79.8(+1.8)	+76.5	+10.6(+0.3)	+221.7	+89.9(−4.2)
AB_3	''$Z3$''	−27.9(+0.7)	+96.8	+56.9(−0.2)	+50.0	−28.2(+1.8)	+142.0	+32.4(+4.0)
A_2B_2	''$Z2$''	−28.8(−0.3)	+164.7	+77.8(+0.4)	+136.4	−6.7(−1.0)	+286.7	+70.2(+0.1)
A_2B_3	''$Z5$''						+273.3	+57.1(−0.8)
A_3B_3	''$Z6$''						+355.5	+63.2(+0.7)
$A_\infty B_\infty$		0.0(0.0)		+20.4(0.0)		+20.3(−0.1)	+576.2	+30.8(0.0)
(111) Structures								
AB	$L1_1$	−43.0(−0.4)	+134.8	+129.8(−1.1)	+60.3	+32.5(−0.1)	+192.3	+166.8(+1.4)
A_2B	''$\alpha 1$''	−30.2(0.0)	+152.4	+120.4(−2.9)	+123.0	+61.4(−7.7)	+288.5	+202.2(−6.4)
AB_2	''$\alpha 2$''	−30.8(0.0)	+124.9	+95.0(+2.9)	+86.4	+2.1(+7.7)	+200.9	+100.9(+6.4)
A_3B	''$V1$''	−21.3(+0.3)	+145.9	+108.4(+0.4)	+136.1	+78.6(+4.1)	+290.8	+193.7(+4.1)
AB_3	''$V3$''	−21.4(+0.6)	+106.8	+73.6(+1.5)	+79.5	+5.1(+0.8)	+172.8	+83.0(+4.0)
A_2B_2	''$V2$''	−22.9(−0.4)	+177.1	+109.1(−1.0)	+170.6	+52.2(−2.5)	+335.8	+162.4(−4.1)
$A_\infty B_\infty$		0.0(0.0)		+86.3(−1.0)		+95.8(+0.3)	+576.2	+173.8(+1.3)
(011) Structures								
A_2B	$\gamma 1$	−49.7(−0.4)	+106.4	+100.3(−0.6)	−14.2	−18.4(+3.3)	+123.3	+98.9(−3.8)
AB_2	$\gamma 2$	−46.9(+0.4)	+97.2	+92.5(+0.8)	+1.7	−6.7(−5.2)	+126.3	+102.6(+3.8)
A_3B	''$Y1$''	−37.0(0.0)	+105.1	+85.4(+3.5)	+21.8	−1.3(+3.8)	+148.5	+99.2(+7.8)
AB_3	''$Y3$''	−35.4(+0.6)	+85.5	+75.2(−1.3)	+19.4	−1.0(+0.1)	+104.1	+78.7(+1.1)
A_2B_2	''$Y2$''	−44.1(−0.3)	+136.0	+105.7(−1.1)	+59.5	−4.2(−2.0)	+192.3	+96.6(−4.5)
$A_\infty B_\infty$		0.0(0.0)		+75.3(−1.2)		+66.1(+0.3)	+576.2	+117.7(+1.6)
(113) Structures								
A_3B	''$W1$''	−35.9(+0.5)	+104.7	+94.2(−0.2)	+22.0	+7.0(+1.5)	+125.7	+120.8(+5.2)
AB_3	''$W3$''	−34.4(−0.2)	+98.6	+91.4(+9.0)	+21.1	+7.8(+0.6)		+88.4(+5.3)
A_2B_2	''$W2$''	−50.6(−0.1)	+121.9	+104.7(−4.4)	+15.7	−20.9(−1.0)	+144.2	+93.6(−5.3)
$A_\infty B_\infty$		0.0(0.0)		+65.9(−1.4)		+69.5(+0.4)	+576.2	+119.8(+1.9)
(201) Structures								
A_3B	$D0_{22}$	−42.3(−0.2)	+85.2	+85.1(+1.3)	−32.7	−32.8(+0.3)	+75.0	+75.0(+5.6)
AB_3	$D0_{22}$	−41.0(−0.3)	+76.8	+76.4(−0.5)	−10.6	−11.8(−1.8)	+68.7	+68.6(+1.5)
A_2B_2	CH or ''40''	−55.3(+0.3)	+109.6	+107.5(−0.4)	−19.0	−23.0(−0.6)	+93.5	+84.8(−3.6)
$A_\infty B_\infty$		0.0(0.0)		+67.3(+1.6)		+53.4(−0.4)	+576.2	+84.8(−2.0)
(401) Structure								
A_5BAB	$D0_{23}$				−33.3	−33.6(0.0)		
(601) Structure								
A_5BAB	LPS-3				−34.1			

TABLE III. (*Continued.*)

Structure		Ag-Au	Cu-Ag		Cu-Au		Ni-Au	
Superlattice	Name	$\Delta H^{\mathrm{LDA}}_{\mathrm{unrel}}$	$\Delta H^{\mathrm{LDA}}_{\mathrm{unrel}}$	$\Delta H^{\mathrm{LDA}}_{\mathrm{rel}}$	$\Delta H^{\mathrm{LDA}}_{\mathrm{unrel}}$	$\Delta H^{\mathrm{LDA}}_{\mathrm{rel}}$	$\Delta H^{\mathrm{LDA}}_{\mathrm{unrel}}$	$\Delta H^{\mathrm{LDA}}_{\mathrm{rel}}$
Other Structures								
A_3B	$L1_2$	$-43.4(+0.4)$	$+84.8$	$+84.8(-1.4)$	-37.3	$-37.3(-0.1)$	$+77.5$	$+77.5(-2.7)$
AB_3	$L1_2$	$-44.0(+0.3)$	$+76.0$	$+76.0(+1.8)$	-17.3	$-17.3(-0.8)$	$+78.9$	$+78.9(-0.2)$
A_7B	$D7$	$-20.8(+0.6)$	$+61.9$	$+61.9(-3.1)$	$+6.8$	$+6.8(-8.3)$	$+82.9$	$+82.9(-15.8)$
A_4B_4	$D4$	$-42.9(+1.1)$						
AB_7	$D7_b$	$-20.0(-0.1)$	$+47.1$	$+47.1(-3.3)$	$+12.9$	$+12.9(+1.9)$	$+56.8$	$+56.8(-0.7)$
A_8B	Ni_8Nb-type		$+63.7$	$+47.7(+0.4)$	$+9.3$	$-9.1(-4.5)$		
AB_8	Ni_8Nb-type		$+42.7$	$+36.4(-1.7)$	$+30.9$	$+18.2(+13.3)$		
Random								
A_4B_4	$SQS8_a$	$-42.5(+0.2)$				$+12.9(+5.7)$		$+122.6(+1.2)$
A_4B_4	$SQS8_b$	$-43.6(-0.2)$				$-15.2(-5.7)$		$+97.5(-9.7)$
A_3B	$SQS14_a$		$+116.2$	$+77.3(+7.0)$	$+56.5$	$+5.5(+7.7)$	$+183.2$	$+96.8(+15.3)$
AB_3	$SQS14_b$		$+92.2$	$+69.7(-7.0)$	$+37.8$	$-5.2(-7.7)$	$+118.2$	$+59.8(-15.3)$

We have taken $l_{\max}=10$, which gives five composition-dependent fitting coefficients determined from a fit to the directly calculated values [Eq. (14)] for six principal directions. The characteristic errors of this fit at the equiatomic composition are 1–2 meV/atom. Equation (19) is then used in Eqs. (11) and (12).

C. Constructing the cluster expansion

Once we have a closed-form expression for the equilibrium constituent strain energy $\Delta E_{\mathrm{CS}}(\sigma)$ and a set $\{\Delta H^{\mathrm{LDA}}(\sigma)\}$ of $T=0$ formation enthalpies, we determine the unknown cluster interactions of Eq. (10) in the following two-step process.

First, the total energies of all structures from Table III are used in the fit to investigate the behavior of the root-mean-square (rms) error Δ_{rms} of the fit, Eq. (13), as a function of the number of real-space pair and multibody interactions. Reciprocal-space CE allows one to add pair interactions systematically in the order of increasing intersite separation, up to any number of near-neighbor shells. The **k**-space smoothness criterion in Eq. (13) automatically selects optimally short-ranged interactions and chooses physically important pair interactions which are essential to produce a good fit to the directly calculated LDA energies. The dependence of the rms error on the number of pair and multibody interactions is shown in Fig. 4. Figure 4(a) is obtained by fixing the number of multibody interactions and varying the number of pair interactions. It shows that in all systems the cluster expansion is well converged using 10–20 pair interactions. The convergence rate is fastest for Ag-Au and slowest for Ni-Au, which we attribute to increasing size mismatch going from Ag-Au to Ni-Au, with Cu-Ag and Cu-Au exhibiting intermediate convergence rates.

The selection of important multibody interactions is more delicate. The number of pair interactions is fixed to a converged value (20 or more), and a large set of three to four-body figures is tested as to whether it improves the rms error

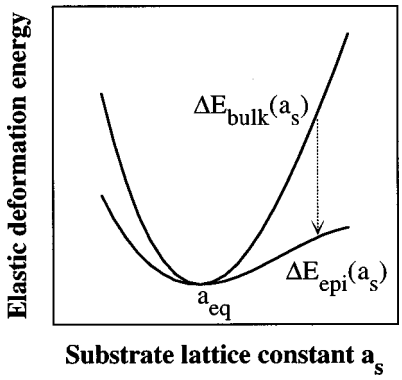

FIG. 1. A schematic illustration of the concept of the epitaxial softening function $q(\hat{G})$, given by the ratio of the bulk (upper curve) and epitaxial (lower curve) deformation energies. In the harmonic approximation $q(\hat{G})$ is the ratio of the curvatures of these curves at the equilibrium point.

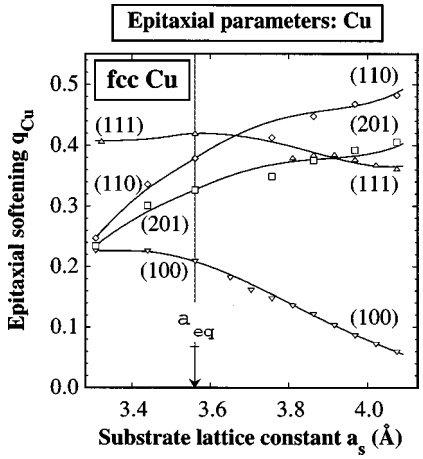

FIG. 2. $q(\hat{G})$ of fcc Cu for principle directions as functions of the substrate lattice parameter a_s. Directly calculated LDA values are represented by open symbols, and lines show the fit using the expansion of $\gamma(\hat{G})$ in Kubic harmonics.

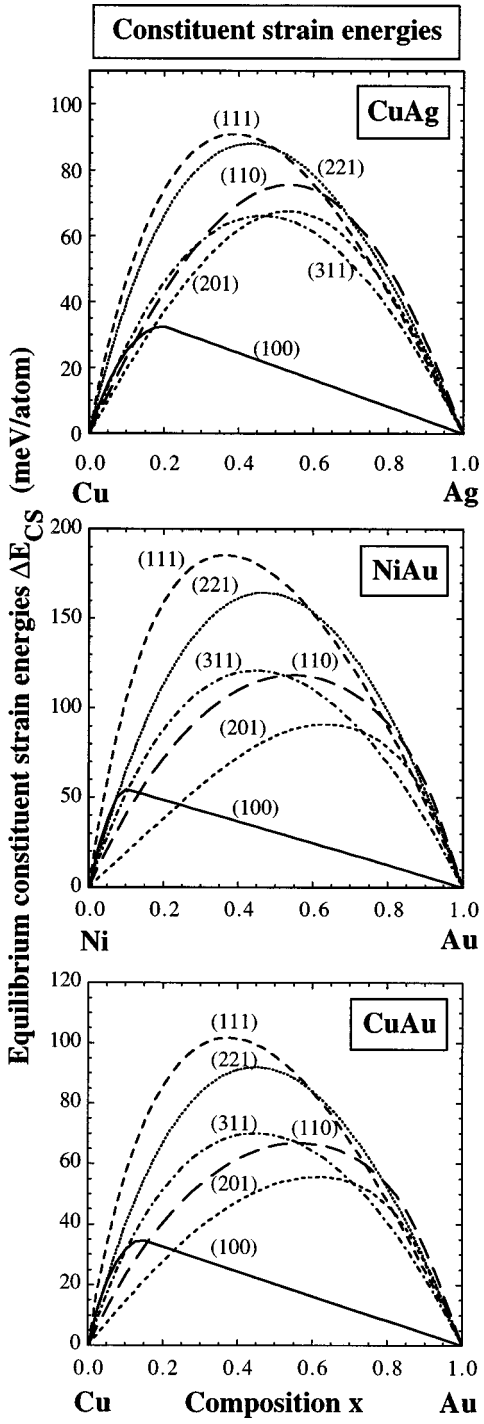

FIG. 3. Equilibrium constituent strain energies for Cu-Au, Ni-Au, and Cu-Ag. The constituent strain energy of Ag-Au is negligibly small and therefore not shown.

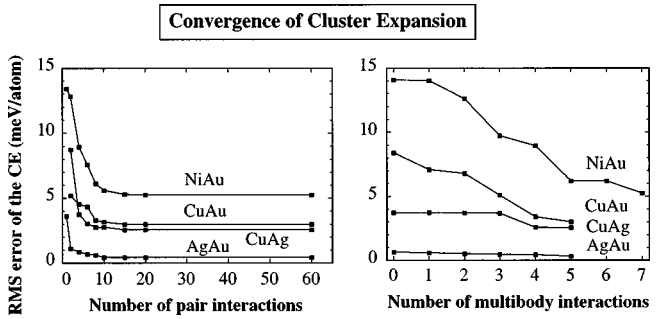

FIG. 4. Root-mean-square errors Δ_{rms} of the cluster expansions for Ag-Au, Cu-Ag, Cu-Au, and Ni-Au as functions of the number of pair and multibody interactions.

of the overall fit. It is retained in the CE only if Δ_{rms} decreases considerably. During the fitting process, we also monitor the overall stability of the CE, as measured by a change in other multibody interactions upon the addition of a particular figure. Unstable behavior usually signals the presence of linear dependences in the chosen set of clusters and an ill-conditioned inverse problem, necessitating a different choice of $\{J_f\}$. Figure 4(b) shows the convergence of the CE with respect to the number of multibody interactions, keeping N_{pairs} equal to their converged values. An important thing to notice is that the multibody interactions produce a decrease in the rms error which is of the same magnitude as that due to the pair interactions. Furthermore, the effect of multibody interactions is largest in Ni-Au, and decreases in order of decreasing size mismatch, becoming negligible in Ag-Au.

In the second step we test the stability of the fit and its predictive power. Using the trial set of figures obtained in the previous step, we exclude several structures which are fit rather well (e.g., $Z2$, $\beta 2$, and $L1_2$ in Ni-Au), and repeat the fit, obtaining new values of the effective cluster interactions. These values are used to predict the total energies of the structures excluded from the fit. If the change in $\Delta H_{\mathrm{CE}}(\sigma)$ is not acceptable (more than few meV/atom), we return to the first step to search for a better set of interactions. The most severe test is to exclude structures with the poorest fit to their formation enthalpies, e.g., $\mathrm{SQS14}_a$ and $\mathrm{SQS14}_b$ in Ni-Au. If the predicted formation energy does not change significantly, the chosen set of figures is considered to be stable and predictive. The final cluster expansion is produced by using this set of figures and all structures from Table III.

Figure 5 shows the calculated pair interactions as function of the near-neighbor fcc shell. There are several noteworthy trends in the four alloy systems.

(i) Only in Ag-Au and Cu-Au are the nearest-neighbor pair interactions dominant: in Cu-Ag the first and third neighbor pair interactions are of similar magnitude, while the third neighbor interaction dominates in Ni-Au.

(ii) The dominant interactions have signs consistent with the observed phase diagrams: Ag-Au and Cu-Au have positive (''antiferromagnetic'') nearest-neighbor pair interactions J_2, corresponding to the tendency towards complete miscibility and ordering at low temperatures. The behavior of Ni-Au, in spite of *positive* first and second neighbor pair interactions, is dominated by the ''ferromagnetic'' third neighbor interaction L_2 (which causes phase separation at low temperatures). Both dominant first and third neighbor pair interactions in Cu-Ag are negative, implying a miscibility gap. The constituent strain energy $\Delta E_{\mathrm{CS}}^{\mathrm{eq}}$ is always positive and therefore increases the propensity for incoherent phase separation.

(iii) Although the nearest-neighbor pair interaction is clearly dominant in Cu-Au, other pair interactions show a long-ranged oscillatory behavior extending over approximately 15 shells. As found in other systems,[65,85] this is a direct consequence of the atomic relaxation caused by the

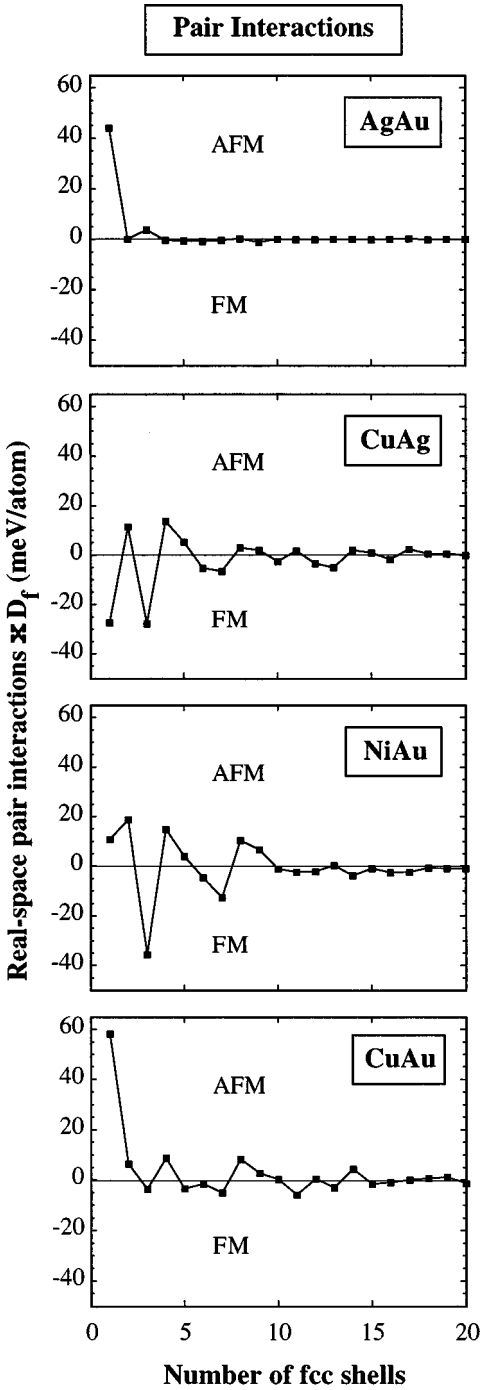

FIG. 5. Real-space pair interactions for the studied noble-metal alloy systems.

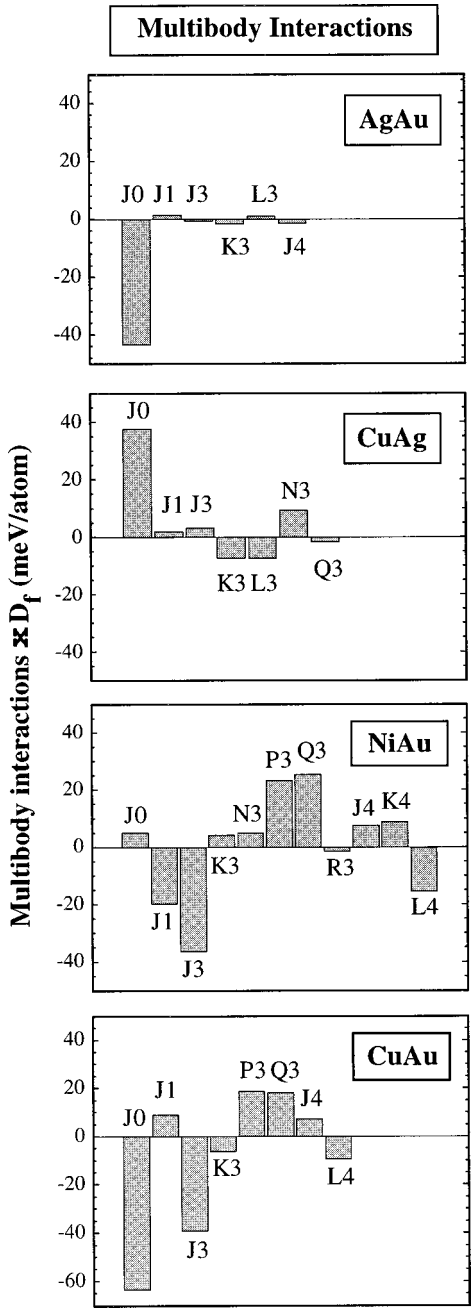

FIG. 6. Multibody interactions for the studied noble-metal alloy systems.

constituent size mismatch between Cu and Au. The pair interactions are slowly decaying in Cu-Ag and Ni-Au, too.

The calculated multibody interaction energies are shown in Fig. 6. J_1 is the point interaction, J_3, K_3, N_3, ... are triplets and J_4, K_4, and L_4 are four-point clusters in increasing order of interatomic separation (see Lu *et al.*[54] for a full description of the clusters). Figure 6 illustrates the importance of the multibody terms in our Hamiltonian.

D. Finding the $T=0$ ground states and $T>0$ properties

Having parametrized the configurational energies in terms of the mixed-space cluster expansion, Eq. (10), we can use it with established statistical methods to predict various structural properties: $T=0$ ground states, order-disorder transition temperatures, configurational entropies, free energies, phase stabilities, and atomic short-range order parameters. Due to the presence of both reciprocal- and real-space terms in the Hamiltonian (10), traditional techniques, e.g., the cluster variation method, are not readily applicable. Monte Carlo simulations must be used instead to calculate statistical properties at finite temperatures. The basic computational algorithm is as follows. We adopt the Metropolis algorithm in the canonical ensemble (fixed composition). For each attempted spin flip, the change in the multiplet interaction energy is evaluated in the real space. To obtain the reciprocal-space energy (constituent strain and pair interaction energies), the Fourier transform of the spin function $S(\mathbf{R}_i,\sigma)$ is needed. It

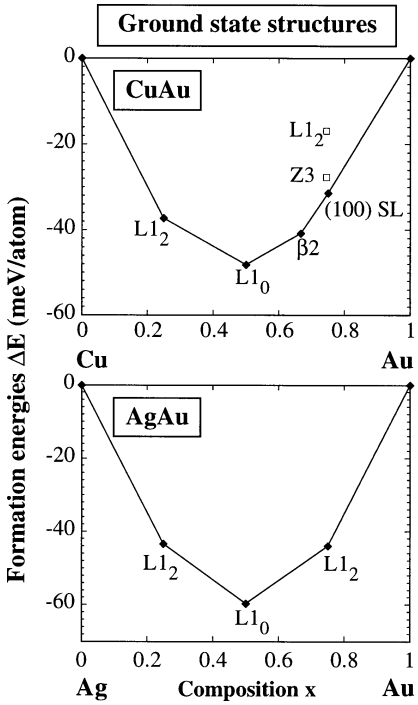

FIG. 7. $T=0$ K ground state lines for Cu-Au and Ag-Au obtained from simulated annealing calculations. $L1_2$ $CuAu_3$ is not only above the ground state line, but also has a higher formation enthalpy than other structures at the same composition; e.g., LDA calculations place the formation enthalpy of $Z3$ below that of $L1_2$. Plots for Cu-Ag and Ni-Au are not shown since these systems phase separate at $T=0$ K.

can be calculated either with the help of the fast Fourier transform (FFT) or evaluated directly taking advantage of the special method described in Ref. 87. The latter is much more economical: If the total number of sites in the simulation box is N, a full FFT has to be done only once after approximately every $\sqrt{N}$ accepted spin flips, which makes the whole computational effort for this special method scale as $N^{1.5}$.

A simulation box of $N=4096$ atoms ($16\times16\times16$) is used to calculate all thermodynamic properties presented in this paper. The transition temperatures are computed by cooling the system from high temperatures and monitoring the discontinuities in the average energy and peaks in heat capacity. To eliminate possible hysteresis effects, the resulting low-temperature configurations are gradually heated up past the transition point. The former process provides the lower bound on the transition temperature T_1, while the latter gives the upper bound T_2. The heating and cooling rates are such that T_1 and T_2 differ by no more than 20 K, an insignificant uncertainty compared to the inaccuracies of the LDA calculations and the fit errors of the cluster expansion. Here 1000 flips/site and a temperature decrease of 2% for each Monte Carlo step are usually sufficient, although in a few cases the results are checked using 2000 flips/site and 0.5% temperature change.

Zero-temperature ground states are found by cooling the system to $T=0$ and checking whether the energy of the final configuration lies on the convex hull. This process is repeated for several random number seeds and starting temperatures, always yielding configurations with similar (usually identical) energies. We explore many equally spaced compositions with an interval $\Delta x=0.05$. The number of possible configurations for each x is $N_{\text{conf}}=N!/(xN)![N(1-x)]!$.

The configurational entropy of the disordered alloys at finite T is computed from the energy vs temperature curves obtained by cooling the system from very high (''$T=\infty$'') temperatures. The following thermodynamic formula gives the configurational entropy at temperature T:

$$\Delta S_{\text{conf}}(T)=\Delta S_{\text{ideal}}+E(T)/T-k_B\int_0^{\beta}E(\beta')\,d\beta', \quad (20)$$

where $\beta=1/k_BT$ and $\Delta S_{\text{ideal}}=k_B[x\ln x+(1-x)\ln(1-x)]$ is the configurational entropy of an ideal solid solution.

IV. RESULTS

A. $T=0$ ground states

1. Ground states of Cu-Au

Figure 7 shows the calculated $T=0$ ground state lines of Cu-Au and Ag-Au which were obtained from simulated annealing quenches of a $16\times16\times16$ system. In Cu-Au, we find the $L1_2$ (Cu_3Au) and $L1_0$ (CuAu) structures as the stable ground states of Cu-rich alloys, in agreement with the existing phase diagram data.[1–4] These data also list $L1_2$ as the stable low-temperature phase of $CuAu_3$. However, we find new, previously unsuspected ground states of Au-rich compounds, all belonging to the family of (001) superlattices. At $x=\frac{2}{3}$ we find a stable $\beta2$ ($CuAu_2$) phase (prototype $MoSi_2$), which is a $CuAu_2$ superlattice along (001). At $x=\frac{3}{4}$, our cluster expansion predicts that a complex $CuAu_4CuAu_4CuAu_2CuAu_2$ (001) superlattice falls on the convex hull, although its energy is less than 2 meV below the tie line connecting $\beta2$ ($CuAu_2$) and Au. Furthermore, even the directly calculated LDA enthalpy of formation of $Z3$ [which is a $CuAu_3$ (001) superlattice] is considerably lower than that of $L1_2$ $CuAu_3$.

We carefully checked whether the predicted new LDA ground states for Au-rich Cu-Au alloys are artifacts of some approximation in our LDA calculations or the fit error of the cluster expansion. The latter possibility was quickly dismissed, since the directly calculated LDA enthalpies of formation for $L1_0$, $\beta2$, $L1_2$, and $Z3$ agreed with the values derived from the cluster expansion to better than 2 meV/atom (see Table III), while the new (100) SL ground state is 14 meV/atom below $L1_2$. To address the former possibility, we performed careful convergence tests for $L1_0$, $\beta2$, $L1_2$, and $Z3$ with respect to the plane wave cutoff and number of **k** points in the first Brillouin zone. The cutoff was increased from $RK_{\max}=9$ to $RK_{\max}=11$ and the density of the Brillouin zone mesh was doubled from $8\times8\times8$ to $16\times16\times16$, an eightfold increase in the total number of **k** points. These tests showed that the formation enthalpies of $L1_0$, $\beta2$, and $L1_2$ were converged to within 1 meV/atom with respect to the size of the basis set and the number of **k** points. Further, we checked how the choice of muffin-tin radii affected ΔH. Varying R_{MT}(Au) between $2.3a_0$ and $2.5a_0$ changed the formation enthalpies by at most 2 meV/atom and did not shift the relative stabilities of phases.[102] Finally, we repeated

these calculations using the Perdew-Zunger[90] parametrization of the Ceperley-Alder[91] LDA functional, as well as the generalized gradient approximation (GGA) of Perdew and Wang,[92] and found insignificant (about 2 meV/atom) changes in the formation enthalpies. Inclusion of the spin-orbit interaction in the second variation procedure[104] changed the formation enthalpy of $L1_0$ (CuAu) by only 3.7 meV/atom (from -48.2 to -51.9), indicating that it is not important for the energetics of Cu-Au. This conclusion is in line with the findings of Ref. 105 that the spin-orbit interaction influences the band structure but has little effect on equilibrium lattice properties. Therefore, we conclude that *state-of-the-art first-principles density functional calculations do not predict $L1_2$ to be a stable $T=0$ ground state of $CuAu_3$*. It is possible that van der Waals interactions, omitted by the LDA and important for large, polarizable atoms such as Au, can affect the formation energies and hence the ground states of Cu-Au.

We next analyze the possibility that the correct $T=0$ ground state around $x=\frac{3}{4}$ is not $L1_2$ as has been assumed in the literature before. Although most compilations[1–4] of binary alloy phase diagrams give $L1_2$ as the stable structure of $CuAu_3$, the experimental evidence[7,8,10] seems inconclusive because of the difficulties in obtaining equilibrated long-range ordered samples. X-ray studies[8] have found superlattice peaks consistent with the cubic $L1_2$ structure, but only very broad low-order reflections have been observed. These superlattice lines could not be sharpened by any heat treatment.[8] It is not clear to us if the x-ray reflections can be reindexed according to some other non-$L1_2$ phase. It is also possible that at elevated ($T\approx 500$ K) temperatures $L1_2$ is stabilized by the entropy (configurational *and* vibrational), while another transformation to the low-energy structure should occur but is kinetically inhibited below 500 K. The biggest experimental obstacles to verifying our predictions seem to be low diffusion rates below the ordering temperature of $CuAu_3$, $T_c\approx 500$ K.

Next we discuss the experimental signatures of the new LDA ground state structures. $MoSi_2$-type $\beta 2$ $CuAu_2$ has a superlattice reflection at $(\frac{2}{3}00)$, but the $CuAu_3$ (100) superlattice has reflections at (100) and $(\frac{1}{3}00)$. These reflections also manifest themselves in the predicted atomic short-range order of the disordered alloys (for details see Ref. 103).

2. Ground states of Ag-Au, Cu-Ag, and Ni-Au

The ground state line of Ag-Au is shown in Fig. 7(b), exhibiting $L1_2$ (Ag_3Au), $L1_0$ (AgAu), and $L1_2$ ($AgAu_3$) stable low-temperature phases. Experimentally, these alloys are known to be completely miscible,[2–4] and there are several indications[69] that they would order below 200 K if not for the very low diffusion rates. Theoretical transition temperatures and short-range order patterns, as well as a complete discussion, are given by Lu, Klein, and Zunger.[54]

The calculated ground states of Cu-Ag and Ni-Au are found to be phase separation, in agreement with the experimental enthalpy data.[2] Neither alloy has a single ordered or disordered structure with negative enthalpy of formation and therefore there are no stable $T=0$ ground states except the phase-separated alloy.

B. Mixing enthalpies

It is interesting to compare the calculated mixing enthalpies of disordered Cu-Au alloys with the available theoretical and experimental data. Table IV summarizes the values of $\Delta H_{\rm mix}(x,T)$ for the completely random ($T=\infty$), short-range ordered ($T=800$ K), and completely ordered ($T=0$ K) Cu-Au alloys at compositions $x=\frac{1}{4}$, $\frac{1}{2}$, and $\frac{3}{4}$. Several important points are apparent from this table.

(i) Studies[50,48,62] which have completely neglected atomic relaxations predict a substantially positive enthalpy of formation for the completely random alloy. In our calculations, relaxations in the random alloy reduce $\Delta H_{\rm mix}(T=\infty)$ by a large amount, bringing it down to essentially zero.

(ii) Comparison of the present results for the $T=\infty$ random alloys with those of Wei *et al.*[51] shows the influence of the number of structures included in the cluster expansion. Since Wei *et al.* used the same FLAPW method,[88] but included a set of only five high-symmetry ordered structures [$A1$ (Cu), $L1_2$ (Cu_3Au), $L1_0$ (CuAu), $L1_2$ ($CuAu_3$), and $A1$ (Au)], the atomic relaxation effects were included incompletely. Indeed, their treatment gives much larger mixing enthalpies of the random Cu-Au alloys than the present work, employing approximately 30 low-symmetry structures with large relaxations. Therefore we conclude that the Connolly-Williams set of five ordered structures cannot correctly capture the large decrease of the mixing enthalpy of random Cu-Au alloys caused by the atomic relaxations.

(iii) The good agreement between the relaxed (this study) and ''unrelaxed'' (Wei *et al.*[51]) values of $\Delta H_{\rm mix}$ at $T=800$ K suggests that the short-range order in Cu-Au tends to decrease the role of the atomic relaxations. This effect can be qualitatively explained on the basis of the ordering tendency towards high-symmetry structures which have little or no relaxation energy ($L1_2$ and $L1_0$ in Cu-rich alloys).

(iv) The mixing enthalpies of the random alloy calculated by Weinberger *et al.*[58] using the CPA differ strongly not only from those obtained using the cluster expansion methods,[51,50,48] but also from the numbers given in the CPA work of Ruban, Abrikosov, and Skriver.[62] Since the CPA of Weinberger *et al.*[58] neglects the (a) atomic relaxation, (b) charge transfer, and (c) short-range order, which all lower the formation energies, the negative values obtained by Weinberger *et al.*[58] are very puzzling.

(v) There are significant discrepancies between the best calculated and experimentally measured[15,14,2] values of $\Delta H_{\rm mix}$ at both $T=0$ K and $T=800$ K. At present these discrepancies are hard to explain since the available general potential LDA calculations[51,52,57] of $\Delta H(L1_2)$ and $\Delta H(L1_0)$ agree with each other reasonably well. On the other hand, the formation energies in Cu-Au are numerically very small and present a severe test for any first-principles model of electronic exchange correlation. It is noteworthy that several less accurate first-principles calculations, using the ASA, have achieved better agreement with the experimental enthalpies of formation than the state-of-the-art general potential techniques. We consider this to be fortuitous. In all cases, LDA calculations correctly predict the relative magnitudes of ΔH for $L1_2$ and $L1_0$, as well as reproduce measured asymmetry in formation enthalpies towards more negative values of $\Delta H_{\rm mix}$ for Cu-rich alloys.

TABLE IV. Calculated mixing enthalpies of disordered $Cu_{1-x}Au_x$ alloys compared with the values obtained by other studies and experimental measurements (in meV/atom). FLAPW is the full-potential linearized augmented plane wave method; LMTO, linearized muffin-tin-orbital method; KKR, Korringa-Kohn-Rostoker multiple scattering method; ASA, atomic-sphere approximation; CPA, coherent potential approximation; CWM, Connolly-Williams cluster expansion; MSCE, mixed-space cluster expansion used in this study; ''Rel.,'' incorporating atomic relaxations; and ''Unrel.,'' neglecting atomic relaxations.

Composition	Expt. [f]	This study FLAPW MSCE (Rel.)	Wei *et al.* [a] FLAPW CWM (Rel.)	Amador and Bozzolo [b] LMTO-ASA CWM (Unrel.)	Terakura *et al.* [c] ASW CWM (Unrel.)	Ruban *et al.* [d] LMTO-ASA CPA (Unrel.)	Weinberger *et al.* [e] KKR-ASA CPA (Unrel.)
$\Delta H_{mix}(T=\infty)$							
$Cu_{0.75}Au_{0.25}$		+2.6	+46.3	+59	+26.9	+54.6	−27
$Cu_{0.50}Au_{0.50}$		+1.6	+38.0	+61	+30.4	+44.3	−57
$Cu_{0.25}Au_{0.75}$		+5.4	+18.6	+39	+20.4	+19.8	−31
$\Delta H_{mix}(T=800\ K)$							
$Cu_{0.75}Au_{0.25}$	−46 [g]	−17.3		−6			
$Cu_{0.50}Au_{0.50}$	−53 [g]	−19.3	−16.9	−5			
$Cu_{0.25}Au_{0.75}$	−31 [g]	−1.2	−2.6	+8			
$\Delta H_{mix}(T=0\ K)$							
$L1_2$ Cu_3Au	−74	−37.3	−36.0		−65.0	−60.7	−54
$L1_0$ CuAu	−91	−48.2	−62.9		−69.7	−83.4	−76
$L1_2$ $CuAu_3$	−59	−17.3	−26.4		−34.0	−56.1	−47

[a]Ref. 51 using the Connolly-Williams structures (relaxation of $L1_0$ only).
[b]Ref. 50.
[c]Ref. 48.
[d]Ref. 62.
[e]Ref. 58.
[f]Ref. 2.
[g]Values obtained at $T=720$ K.

C. Order-disorder transition temperatures

Order-disorder transitions have been investigated at compositions ($x=\frac{1}{4}$, $\frac{1}{2}$, $\frac{2}{3}$, and $\frac{3}{4}$) using the Monte Carlo simulation technique described in Sec. III D. The resulting transition temperatures T_c are given in Table V. All transitions are found to be first order, involving discontinuities in the energy and correlation functions. At $x=\frac{1}{4}$ we find a transition from the disordered state to long-range ordered $L1_2$ Cu_3Au at $T_c=530$ K, which is only 130 K lower than the experimentally observed transition temperature. For the equiatomic alloy at $x=\frac{1}{2}$ the calculated and experimental transition temperatures agree to a few degrees kelvin. However, we do not find the CuAu II phase which exists in a narrow temperature range between 658 K and 683 K. This phase is stabilized by the free energy differences between $L1_0$ and long-period superstructures of $L1_0$ which are as small as 1 meV/atom (Ref. 56) and therefore beyond the accuracy of self-consistent LDA calculations.

For $x=\frac{3}{4}$ we obtain a sequence of transformations, the first one occurring at $T=750$ K from the disordered $A1$ phase to a coherent two-phase mixture of $\beta 2$ and $A1$. Then a subsequent transition at $T=635$ K takes $CuAu_3$ into the long-range ordered (100) superlattice which is predicted to be the stable $T=0$ ground state at that composition (see Sec. IV A 1). The calculated transition at $x=\frac{2}{3}$ goes straight into the $\beta 2$ phase at $T=735$ K. Therefore, a two-phase $\beta 2+A1$ field is predicted to exist at temperatures somewhere between 635 K and 730 K and around $x=\frac{3}{4}$. These predictions reflect the LDA. As stated in Sec. IV A 1, corrections to the LDA might be significant.

D. Nonconfigurational entropy

The effect of the nonconfigurational entropy (electronic, vibrational, etc.) on the alloy phase stability has recently attracted considerable interest.[106–116] For instance, it has

TABLE V. Calculated order-disorder transition temperatures (in K) for Cu-Au. $A1$ denotes the configurationally disordered fcc phase, and n/a means that the transition has not been observed (either experimentally or in the Monte Carlo simulation).

Composition	Transition	Expt.	This study
$x=\frac{1}{4}$	$A1\rightarrow L1_2$	663	530
$x=\frac{1}{2}$	$A1\rightarrow L1_0$	683/658 [a]	660
$x=\frac{2}{3}$	$A1\rightarrow\beta 2$	n/a	735
$x=\frac{3}{4}$	$A1\rightarrow L1_2$	≈500	n/a
	$A1\rightarrow\beta 2+A1$	n/a	750
	$\beta 2+A1\rightarrow(100)$SL	n/a	680

[a]CuAu undergoes a transition to CuAu-II at 683 K, subsequently transforming into $L1_0$ CuAu I at 658 K.

TABLE VI. The experimentally measured (Ref. 2) entropy of formation $\Delta S^{\rm form}_{\rm tot}(T)$, the calculated configurational entropy $\Delta S^{\rm calc}_{\rm conf}$, and the derived nonconfigurational entropy of formation $\Delta S^{\rm form}_{\rm nonconf}(T)$. All values are given in units of k_B/atom.

System	x	T (K)	$\Delta S^{\rm form}_{\rm tot}(T)$	$\Delta S_{\rm ideal}$	$\Delta S^{\rm calc}_{\rm conf}(T)$	$\Delta S^{\rm form}_{\rm nonconf}(T)=\Delta S^{\rm form}_{\rm tot}(T)-\Delta S^{\rm calc}_{\rm conf}(T)$
Cu-Au	0.5	800	0.73	0.69	0.57	0.16
Ag-Au	0.5	800	0.52	0.69	0.62	−0.10
Cu-Ag	0.141	1052	0.77	0.41	0.40 [a]	0.37
Ni-Au	0.5	1100	1.04	0.69	0.56	0.48

[a]This value was obtained at $T=1136$ K, since a coherent phase separation starts at lower temperatures.

been suggested[108–115] that there are large differences in the vibrational *entropies of ordering* $S^{\rm vib}_{\rm ordered}-S^{\rm vib}_{\rm disord}$, which should manifest themselves in shifts of the order-disorder transition temperatures. There is another important class of thermodynamic properties where the vibrational entropy may play a role and which has often been overlooked. Namely, it is the *entropy of formation* with respect to the pure constituents, defined in analogy with ΔH in Eq. (4):

$$\Delta S^{\rm form}_{\rm tot}(A_{1-x}B_x,T)=S(A_{1-x}B_x,T)-(1-x)S(A,T)-xS(B,T), \quad (21)$$

where $S(A,T)$ is the total entropy of the pure constituent A at temperature T. It is often assumed that the configurational entropy is the dominant contribution to $\Delta S^{\rm form}_{\rm tot}(A_{1-x}B_x,T)$ because all other contributions cancel out in Eq. (21). The nonconfigurational entropy of formation,

$$\Delta S^{\rm form}_{\rm nonconf}(A_{1-x}B_x,T)=\Delta S^{\rm form}_{\rm tot}(A_{1-x}B_x,T)-\Delta S_{\rm conf}(A_{1-x}B_x,T), \quad (22)$$

contributes to such important quantities as mutual solubility limits and miscibility gap temperatures.

Noble-metal alloys are excellent cases to test the values of $\Delta S^{\rm form}_{\rm nonconf}$ since accurate experimental data on the entropies of formation, $\Delta S^{\rm form}_{\rm tot}$, are available, and the configurational entropy $\Delta S_{\rm conf}$ can be calculated accurately using the thermodynamic integration technique described in Sec. III D. Table VI gives the measured entropies of formation for disordered solid solutions $A_{1-x}B_x$, $\Delta S^{\rm form}_{\rm tot}(x,T)$, the maximum attainable configurational entropy $\Delta S_{\rm ideal}$, as well as the theoretically calculated configurational entropy $\Delta S^{\rm calc}_{\rm conf}$ and the derived value for the nonconfigurational entropy of formation, $\Delta S^{\rm form}_{\rm nonconf}$. It shows that the size-mismatched noble-metal systems have large amounts of $\Delta S^{\rm form}_{\rm nonconf}$ in the disordered solid solution. Since it is unlikely that these values of $\Delta S^{\rm form}_{\rm nonconf}$ are of electronic or magnetic origin, we suggest that the excess entropy in the disordered solid solutions of Ni-Au, Cu-Ag, and Cu-Au is vibrational. It is possible that the atomic relaxations lead to a softening of lattice vibrations, although the physical mechanism of this softening is unclear at present.

Sanchez *et al.*[49] in their study of the Cu-Ag system noted that even a very crude model of the vibrational entropy markedly improved the agreement with the experimental solubility data. In the case of Ni-Au, which exhibits the largest $\Delta S^{\rm form}_{\rm nonconf}$, it is possible to reconcile the experimentally measured and theoretically calculated miscibility gap temperatures only by taking into account the nonconfigurational entropy of formation.[117]

The fact that Cu-Au also has a positive $\Delta S^{\rm form}_{\rm nonconf}$ has little qualitative effect on the phase diagram since Cu and Au are completely miscible from total energy and configurational entropy considerations alone. Ag-Au is calculated to have a negative $\Delta S^{\rm form}_{\rm nonconf}$, but its value is close to the experimental uncertainty in the measurement of ΔS.

E. Bond lengths in random alloys

Since recent experimental measurements of the composition dependence of interatomic bond lengths in Cu-Au (Ref 24) and Ni-Au (Ref. 23) have found several unusual features, it is interesting to address these trends from first-principles LDA calculations. In the present work we model the atomic positions in the random alloys using special quasirandom structures[118] (SQS's). These periodic structures are designed to reproduced the pair and multibody correlation functions of the perfectly disordered configuration as closely as possible. It has been shown[118] that even small unit cell SQS's can give rather accurate representation of the properties of random alloys. We have performed LDA calculations for 8 atom/cell SQS's at $x=\frac{1}{4}$ (SQS14$_a$), $x=\frac{1}{2}$ (SQS8$_a$,SQS8$_b$), and $x=\frac{3}{4}$ (SQS14$_b$). The atomic positions and cell coordinates have been fully relaxed to minimize the total energy. The results for Cu-Au and Ni-Au interatomic bond lengths are shown in Fig. 8. The main features are the following.

(i) In spite of the different phase diagram properties (Ni-Au phase separates and Cu-Au orders at $T=0$ K), the calculated behavior of bond lengths is very similar, which we attribute to the similar size mismatch in both systems (12% in Cu-Au and 15% in Ni-Au).

(ii) Our calculations give three distinct bond lengths at all compositions, which is also observed experimentally.[23,24] Probably the most interesting feature in Fig. 8 is the crossing of $R_{BB}(x)$ and $R_{AB}(x)$ curves at $x=\frac{3}{4}$ in both systems. The measurements for Cu-Au (Ref. 24) and Ni-Au (Ref. 23) indicate that this may indeed be correct, since the deduced values around this composition are very close and have large error bars.

(iii) Another important feature, observed experimentally and reproduced by our SQS results, is that A-A bonds change much more as x varies from 0 to 1 than B-B bonds when x varies from 1 to 0, suggesting that the compressed bonds become increasingly stiff and the expanded bonds weaken. This behavior can be explained by the asymmetry in

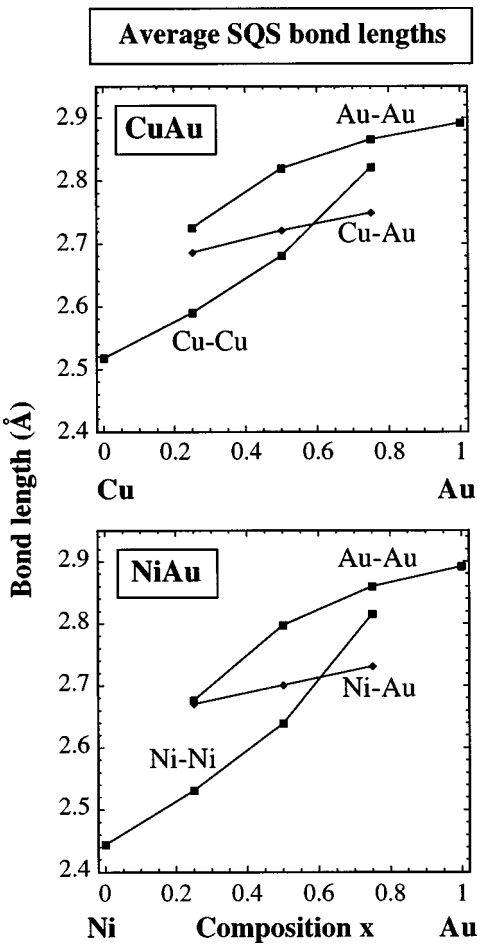

FIG. 8. SQS bond lengths for Cu-Au and Ni-Au.

the interatomic potential curves, which are rapidly hardening upon compression and softening upon expansion. However, our results for R_{AA} at $x=\frac{3}{4}$ and R_{BB} at $x=\frac{1}{4}$ are obtained from an average of only four minority bonds in the SQS14 structures, and perhaps are not representative of a wider statistical sample.

(iv) It is interesting to note that the predicted bond lengths between unlike atoms R_{AB} do not follow the linear relation $R_{AB}=R_{AA}+x(R_{BB}-R_{AA})$.

V. SUMMARY

We have showed that accurate first-principles studies of alloys with large size mismatches are now feasible using the mixed-space cluster expansion method. This method has been applied to noble-metal alloys where vast amounts of experimental data and many theoretical studies are available.

(i) The mixed-space cluster expansion has been generalized to include the effects of nonlinear strain on the formation energies of long-period superlattices. We find that the elastic energy, required to lattice match Cu and Ni to (100) surfaces of Au and Ag, is anomalously low, leading to a very low constituent strain energy of (100) superlattices. This effect is partly responsible for the stabilization of additional LDA ground states of Au-rich Cu-Au alloys.

(ii) In Au-rich Cu-Au, we predict new $T=0$ K ground states. Our LDA results place $L1_2$ ($CuAu_3$), previously thought of as the stable $T=0$ state of $CuAu_3$, higher in energy than a family of superlattices along (100) direction. In particular, $MoPt_2$-type $CuAu_2$ [Cu_1Au_2 superlattice along (100)] and a complicated $CuAu_4CuAu_4CuAu_2CuAu_2$ (100) superlattice are found to be the LDA ground states.

(iii) There are significant discrepancies (up to 50%) between the experimentally measured and calculated LDA mixing enthalpies for Cu-Au alloys. This is surprising since the experimental mixing enthalpies of Ni-Au and Ag-Au are reproduced very well.[54,117]

(iv) The calculated order-disorder transition temperatures are in an excellent agreement with experiment. For instance, $T_c^{\mathrm{calc}}(x=\frac{1}{4})=530$ K and $T_c^{\mathrm{calc}}(x=\frac{1}{2})=660$ K, compared with $T_c^{\mathrm{expt}}(x=\frac{1}{4})=663$ K and $T_c^{\mathrm{expt}}(x=\frac{1}{2})=683/658$ K.

(v) From the experimentally measured entropies of formation $\Delta S_{\mathrm{tot}}^{\mathrm{form}}$ and the calculated configurational entropies $\Delta S_{\mathrm{conf}}^{\mathrm{calc}}$, we obtain large nonconfigurational (probably vibrational) entropies of formation in the size-mismatched systems, $\Delta S_{\mathrm{nonconf}}^{\mathrm{form}}=\Delta S_{\mathrm{tot}}^{\mathrm{form}}-\Delta S_{\mathrm{conf}}^{\mathrm{calc}}$. These entropies allow one to reconcile the experimental miscibility gap temperature and formation enthalpies of Ni-Au with the theoretical LDA values.[117]

(vi) Bond length distributions in Ni-Au and Cu-Au have been studied via supercell calculations employing the special quasirandom structure technique. The important qualitative features of recent EXAFS measurements[23,24] are correctly reproduced: existence of distinct A-A, B-B, and A-B bond lengths at all compositions, possible crossing of $R_{AA}(x)$ and $R_{AB}(x)$ around $x=\frac{3}{4}$ (where x is the composition of the larger constituent), softening of the shorter bond as $x\rightarrow 1$, and deviations of the bond length $R_{AB}(x)$ between unlike atoms from the linear Vergard's law.

ACKNOWLEDGMENTS

This work was supported by the Office of Energy Research, Basic Energy Sciences, Materials Science Division, U.S. Department of Energy, under Contract No. DE-AC36-83CH10093.

[1] *Phase Diagrams of Binary Copper Alloys*, edited by P. R. Subramanian, D. J. Chakrabarti, and D. E. Laughlin (ASM International, Materials Park, OH, 1994).

[2] R. Hultgren, P. D. Desai, D. T. Hawkins, M. Gleiser, and K. Kelley, *Selected Values of the Thermodynamic Properties of Binary Alloys* (American Society for Metals, Metals Park, OH, 1973).

[3] M. Hansen, *Constitution of Binary Alloys* (Genium, Schenectady, NY, 1985).

[4] T. B. Massalski, *Binary Alloy Phase Diagrams* (ASM International, Materials Park, OH, 1990).

[5] *Noble Metal Alloys*, edited by T. B. Massalski (The Metallurgical Society, Warrendale, PA, 1986).

[6] J. M. Cowley, J. Appl. Phys. **21**, 24 (1950).

[7] S. Ogawa and D. Watanabe, J. Appl. Phys. **22**, 1502 (1951).
[8] B. W. Batterman, J. Appl. Phys. **28**, 556 (1957).
[9] G. C. Kuczynski, M. Doyama, and M. E. Fine, J. Appl. Phys. **27**, 651 (1956).
[10] R. Kubiak and J. Janczak, J. Alloys Compd. **176**, 133 (1991).
[11] F. M. d'Heurle and P. Gordon, Acta Metall. **9**, 304 (1961).
[12] R. L. Orr, J. Luciat-Labry, and R. Hultgren, Acta Metall. **8**, 431 (1960).
[13] R. A. Oriani, Acta Metall. **2**, 608 (1954).
[14] R. A. Oriani and W. K. Murphy, J. Phys. Chem. **62**, 327 (1958).
[15] R. L. Orr, Acta Metall. **8**, 489 (1960).
[16] M. Hirabayashi, S. Nagasaki, and H. Kōno, J. Appl. Phys. **28**, 1070 (1957).
[17] M. Bienzle, T. Oishi, F. Sommer, and K. Ono, Mater. Trans. JIM **33**, 51 (1992).
[18] M. Bienzle, T. Oishi, and F. Sommer, J. Alloys Compd. **220**, 182 (1995).
[19] T. Claeson and J. B. Boyce, Phys. Rev. B **29**, 1551 (1984).
[20] G. S. Sohal, C. Carbone, E. Kisker, S. Krummacher, A. Fattah, W. Uselhoff, R. C. Albers, and P. Weinberger, Z. Phys. B **78**, 295 (1990).
[21] T.-U. Nahm, K.-H. Park, S.-J. Oh, S.-M. Chung, and G. K. Wertheim, Phys. Rev. B **52**, 16 466 (1995).
[22] T. Shinohara, S. Saitoh, F. Wagatuma, and S. Yamaguchi, Philos. Mag. Lett. **74**, 153 (1996).
[23] G. Renaud, N. Motta, F. Lançon, and M. Belakhovsky, Phys. Rev. B **38**, 5944 (1988).
[24] A. I. Frenkel, E. A. Stern, A. Rubshtein, A. Voronel, and Yu. Rosenberg, J. Phys. IV **7** (C2), 1005 (1997).
[25] W. Shockley, J. Chem. Phys. **6**, 130 (1938).
[26] J. M. Cowley, Phys. Rev. **77**, 669 (1950).
[27] C. M. van Baal, Physica (Amsterdam) **64**, 571 (1973).
[28] N. S. Golosov, L. E. Popov, and L. Ya. Pudan, J. Phys. Chem. Solids **34**, 1149 (1973); **34**, 1157 (1973).
[29] R. Kikuchi, J. Chem. Phys. **60**, 1071 (1974).
[30] D. de Fontaine and R. Kikuchi, Natl. Bur. Stand. (U.S.) Misc. Publ. No. SP-496 (U.S. GPO, Washington, D.C., 1977), p. 999.
[31] R. Kikuchi, J. M. Sanchez, D. de Fontaine, and H. Yamauchi, Acta Metall. **28**, 651 (1980).
[32] C. Sigli and J. M. Sanchez, Acta Metall. **33**, 1097 (1985).
[33] R. Kikuchi, *Noble Metal Alloys* (The Metallurgical Society, Warrendale, PA, 1986).
[34] W. A. Oates, P. J. Spencer, and S. G. Fries, CALPHAD: Comput. Coupling Phase Diagrams Thermochem. **20**, 481 (1996).
[35] D.-H. Wu and R. A. Tahir-Kheli, J. Phys. Soc. Jpn. **31**, 641 (1971).
[36] B. Chakraborty and Z. Xi, Phys. Rev. Lett. **68**, 2039 (1992).
[37] A. Chiolero, Ph.D. thesis, University of Fribourg, Switzerland, 1995.
[38] B. Chakraborty, Europhys. Lett. **30**, 531 (1995).
[39] G. J. Ackland and V. Vitek, Phys. Rev. B **41**, 10 324 (1990).
[40] H. M. Polatoglou and G. L. Bleris, Interface Sci. **2**, 31 (1994).
[41] G. Bozzolo, J. Ferrante, and J. R. Smith, Phys. Rev. B **45**, 493 (1992).
[42] G. Mazzone, V. Rosato, and M. Pintore, Phys. Rev. B **55**, 837 (1997).
[43] C. Seok and D. W. Oxtoby, J. Phys.: Condens. Matter **9**, 87 (1997).
[44] L. G. Ferreira and M. A. Boselli, Solid State Commun. **96**, 745 (1995).
[45] L. G. Ferreira and M. A. Boselli, J. Phys.: Condens. Matter **9**, 4801 (1997).
[46] M. Ahlers, Z. Phys. B **99**, 491 (1996).
[47] F. Cleri and V. Rosato, Philos. Mag. Lett. **67**, 369 (1993).
[48] K. Terakura, T. Oguchi, T. Mohri, and K. Watanabe, Phys. Rev. B **35**, 2169 (1987); T. Mohri, K. Terakura, S. Takizawa, and J. M. Sanchez, Acta Metall. **39**, 493 (1991).
[49] J. M. Sanchez, J. P. Stark, and V. L. Moruzzi, Phys. Rev. B **44**, 5411 (1991).
[50] C. Amador and G. Bozzolo, Phys. Rev. B **49**, 956 (1994).
[51] S.-H. Wei, A. A. Mbaye, L. G. Ferreira, and Alex Zunger, Phys. Rev. B **36**, 4163 (1987).
[52] Z. W. Lu, S.-H. Wei, A. Zunger, S. Frota-Pessoa, and L. G. Ferreira, Phys. Rev. B **44**, 512 (1991).
[53] Z.-W. Lu and A. Zunger, Phys. Rev. B **50**, 6626 (1994).
[54] Z. W. Lu, B. M. Klein, and A. Zunger, Model. Simul. Mater. Sci. Eng. **3**, 753 (1995).
[55] Z. W. Lu, B. M. Klein, and A. Zunger, Superlattices Microstruct. **18**, 161 (1995).
[56] A. T. Paxton and H. M. Polatoglou Phys. Rev. Lett. **78**, 270 (1996).
[57] J. W. Davenport, R. E. Watson, and M. Weinert, Phys. Rev. B **37**, 9985 (1988).
[58] P. Weinberger, V. Drchal, L. Szunyogh, J. Fritscher, and B. I. Bennett, Phys. Rev. B **49**, 13 366 (1994).
[59] D. D. Johnson and F. J. Pinski, Phys. Rev. B **48**, 11 553 (1993).
[60] J. Kudrnovský, S. K. Bose, and O. K. Andersen, Phys. Rev. B **43**, 4613 (1991).
[61] I. A. Abrikosov, Yu. H. Vekilov, and A. V. Ruban, Phys. Lett. A **154**, 407 (1991).
[62] A. V. Ruban, I. A. Abrikosov, and H. L. Skriver, Phys. Rev. B **51**, 12 958 (1995).
[63] B. Ginatempo and J. B. Staunton, J. Phys. F **18**, 1827 (1988).
[64] P. Hohenberg and W. Kohn, Phys. Rev. **136**, 864 (1964); W. Kohn and L. J. Sham, *ibid.* **136**, A1133 (1965).
[65] D. B. Laks, L. G. Ferreira, S. Froyen, and A. Zunger, Phys. Rev. B **46**, 12 587 (1992).
[66] A. Zunger, in *Statics and Dynamics of Alloy Phase Transformations*, Vol. 319 of NATO Advanced Study Institute, Series B: Physics, edited by P. E. A. Turchi and A. Gonis (Plenum Press, New York, 1994), p. 361.
[67] W. B. Pearson, *Handbook of Lattice Spacings and Structures of Metals and Alloys* (Pergamon, Oxford, 1967).
[68] L. Pauling, *The Nature of the Chemical Bond*, 3rd ed. (Cornell University Press, New York, 1960), p. 93.
[69] B. Schönfeld, J. Traube, and G. Kostorz, Phys. Rev. B **45**, 613 (1992); N. Norman and B. E. Warren, J. Appl. Phys. **22**, 483 (1951); K. Ziesemer, Ph.D. thesis, Universität Frankfurt, 1976.
[70] B. Velický, S. Kirkpatrick, and H. Ehrehreich, Phys. Rev. **175**, 747 (1968); P. Soven, *ibid.* **178**, 1136 (1969).
[71] For a review of the coherent potential approximation, see B. L. Gyorffy, D. D. Johnson, F. J. Pinski, D. M. Nicholson, and G. M. Stocks, in *Alloy Phase Stability*, edited by G. M. Stocks and A. Gonis (Kluwer, Dordrecht, 1898), p. 293.
[72] F. Ducastelle, *Order and Phase Stability in Alloys* (North-Holland, New York, 1991).
[73] Z. W. Lu, S.-H. Wei, and A. Zunger, Phys. Rev. B **45**, 10 314 (1992).
[74] N. Mousseau and M. F. Thorpe, Phys. Rev. B **45**, 2015 (1992).
[75] N. Papanikolaou, N. Stefanou, R. Zeller, and P. H. Dederichs, Phys. Rev. B **55**, 4157 (1997); Comput. Mater. Sci. **8**, 131

(1997); N. Papanikolaou, N. Stefanou, R. Zeller, and P. H. Dederichs, in *Stability of Materials*, Vol. 355 of NATO Advanced Study Institute, Series B: Physics, edited by A. Gonis, P. E. A. Turchi, and J. Kudrnovsky (Plenum, New York, 1996).

[76] Z. W. Lu, S.-H. Wei, and A. Zunger, Phys. Rev. B **44**, 10 470 (1991).

[77] Z. W. Lu, S.-H. Wei, and A. Zunger, Phys. Rev. Lett. **66**, 1753 (1991); **68**, 1961 (1992).

[78] J. W. D. Connolly and A. R. Williams, Phys. Rev. B **27**, 5169 (1983).

[79] D. de Fontaine, in *Solid State Physics*, edited by H. Ehrenreich and D. Turnbull (Academic Press, New York, 1994), Vol. 51.

[80] J. M. Sanchez, F. Ducastelle, and D. Gratias, Physica A **128**, 334 (1984).

[81] M. Asta, C. Wolverton, D. de Fontaine, and H. Dreyssé, Phys. Rev. B **44**, 4907 (1991).

[82] J. M. Sanchez, Phys. Rev. B **48**, 14 013 (1993).

[83] M. Born and K. Huang, *Dynamical Theory of Crystal Lattices* (Oxford University Press, London, 1961).

[84] A. A. Maradudin, E. W. Montroll, G. H. Weiss, and I. P. Ipatova, in *Theory of Lattice Dynamics in the Harmonic Approximation*, in *Solid State Physics*, edited by H. Ehrenreich and D. Turnbull (Academic Press, New York, 1971), Suppl. 3.

[85] S. de Gironcoli, P. Giannozzi, and S. Baroni, Phys. Rev. Lett. **66**, 2116 (1991); M. Peressi and S. Baroni, Phys. Rev. B **49**, 7490 (1994).

[86] K. Binder and D. W. Heerman, *Monte Carlo Simulation in Statistical Physics* (Springer-Verlag, Berlin, 1988).

[87] Z.-W. Lu, D. B. Laks, S.-H. Wei, and A. Zunger, Phys. Rev. B **50**, 6642 (1994).

[88] S.-H. Wei and H. Krakauer, Phys. Rev. Lett. **55**, 1200 (1985), and references therein.

[89] E. Wigner, Phys. Rev. **46**, 1002 (1934).

[90] J. P. Perdew and A. Zunger, Phys. Rev. B **23**, 5048 (1981).

[91] D. M. Ceperley and B. J. Alder, Phys. Rev. Lett. **45**, 566 (1980).

[92] J. P. Perdew and Y. Wang, Phys. Rev. B **33**, 8800 (1986); **40**, 3399(E) (1989); J. P. Perdew, in *Electronic Structure of Solids '91*, edited by P. Ziesche and H. Eschrig (Akademie Verlag, Berlin, 1991), p. 11.

[93] S. Froyen, Phys. Rev. B **39**, 3168 (1989).

[94] R. Yu, D. Singh, and H. Krakauer, Phys. Rev. B **43**, 6411 (1991).

[95] P. Villars and L. D. Calvert, *Pearson's Handbook of Crystallographic Data for Intermetallic Phases* (American Society for Metals, Metals Park, OH, 1985).

[96] V. Ozoliņš, C. Wolverton, and A. Zunger, Phys. Rev. B **57**, 4816 (1998).

[97] A. Zunger, in *Handbook of Crystal Growth*, edited by D. T. J. Hurle (Elsevier, Amsterdam, 1994), Vol. 3, p. 997.

[98] J. Hornstra and W. J. Bartels, J. Cryst. Growth **44**, 513 (1978).

[99] E. Anastassakis, J. Appl. Phys. **68**, 4561 (1990); J. Cryst. Growth **114**, 647 (1991).

[100] D. J. Bottomley and P. Fons, J. Cryst. Growth **160**, 406 (1996).

[101] D. M. Wood, J. Vac. Sci. Technol. B **10**, 1675 (1992).

[102] A. G. Khachaturyan, *Theory of Structural Transformations in Solids* (Wiley, New York, 1983).

[103] C. Wolverton, V. Ozoliņš, and A. Zunger, Phys. Rev. B **57**, 4332 (1998).

[104] A. H. MacDonald, W. E. Pickett, and D. D. Koelling, J. Phys. C **13**, 2675 (1980); W. E. Pickett, A. J. Freeman, and D. D. Koelling, Phys. Rev. B **23**, 1266 (1981).

[105] S.-H. Wei and A. Zunger, Phys. Rev. B **37**, 8958 (1988).

[106] C. Wolverton and A. Zunger, Phys. Rev. B **52**, 8813 (1995).

[107] R. E. Watson and M. Weinert, Phys. Rev. B **30**, 1641 (1984).

[108] L. J. Nagel, L. Anthony, and B. Fultz, Philos. Mag. Lett. **72**, 421 (1995).

[109] L. Anthony, J. K. Okamoto, and B. Fultz, Phys. Rev. Lett. **70**, 1128 (1993).

[110] B. Fultz, L. Anthony, L. J. Nagel, R. M. Nicklow, and S. Spooner, Phys. Rev. B **52**, 3315 (1995).

[111] L. Anthony, L. J. Nagel, J. K. Okamoto, and B. Fultz, Phys. Rev. Lett. **73**, 3034 (1994).

[112] B. Fultz, L. Anthony, J. L. Robertson, R. M. Nicklow, S. Spooner, and M. Mostoller, Phys. Rev. B **52**, 3280 (1995).

[113] L. J. Nagel, B. Fultz, J. L. Robertson, and S. Spooner, Phys. Rev. B **55**, 2903 (1997).

[114] G. D. Garbulsky and G. Ceder, Phys. Rev. B **49**, 6327 (1994); **53**, 8993 (1996).

[115] J. D. Althoff, D. Morgan, D. de Fontaine, M. Asta, S. M. Foiles, and D. D. Johnson, Phys. Rev. B **56**, R5705 (1997).

[116] J. Desplat, F. Bley, and F. Livet, Acta Mater. **44**, 4961 (1996).

[117] C. Wolverton and A. Zunger, Comput. Mater. Sci. **8**, 107 (1997).

[118] A. Zunger, S.-H. Wei, L. G. Ferreira, and J. E. Bernard, Phys. Rev. Lett. **65**, 353 (1990).